LUND UNIVERSITY

Dose-response relationships in neuroendocrine tumours treated with peptide receptor radionuclide therapy

Warfvinge, Carl Fredrik

2026

Document Version:
Publisher's PDF, also known as Version of record

Dose-response relationships in neuroendocrine tumors treated with peptide receptor radionuclide therapy

CARL FREDRIK WARFVINGE
DEPARTMENT OF CLINICAL SCIENCES | FACULTY OF MEDICINE | LUND UNIVERSITY

Dose-response relationships in neuroendocrine tumors treated with peptide receptor radionuclide therapy

Carl Fredrik Warfvinge

LUND
UNIVERSITY

DOCTORAL DISSERTATION

Doctoral dissertation for the degree of Doctor of Philosophy (PhD) at the Faculty of Medicine at Lund University to be publicly defended on 9th of January 2026 at 09.00 in Torsten Landberg-salen, Skåne University Hospital, Klinikgatan 5, Lund.

Faculty opponent
Professor Jonathan Wadsley

University of Sheffield, UK

Organization: LUND UNIVERSITY

Document name: Doctoral dissertation **Date of issue** 2026-01-09

Author(s): Carl Fredrik Warfvinge

Title and subtitle: Dose-response relationships in neuroendocrine tumors treated with peptide receptor radionuclide therapy

Abstract: Neuroendocrine tumors (NET) are malignancies that often express somatostatin receptors, enabling targeted therapy with peptide receptor radionuclide therapy (PRRT). ^{177}Lu- DOTA-TATE improves progression-free survival, yet current protocols apply fixed activity and cycle numbers, despite the possibility of patient-specific dosimetry to quantify ^{177}Lu distribution in organs and tumors. The overarching aim of this thesis was to evaluate whether dosimetry can guide individualized PRRT, to explore absorbed doses to tumors and their relation to patient response.

Data came from the prospective ILUMINET trial, including subsequent post-hoc analyses. Ninety-six patients with advanced grade 1–2 NET received repeated cycles of ^{177}Lu-DOTA-TATE, with number of treatments guided by renal dosimetry. Associations between tumor AD and clinical endpoints were assessed using mixed-effect models, logistic regression, and survival analysis.

Individualization based on renal absorbed dose (AD) allowed most patients to receive more than four cycles without increased renal toxicity and severe adverse events were rare. Tumor AD decreased across cycles, particularly in grade 2 tumors, reflecting reduced uptake over time. Higher cumulative tumor AD correlated with greater tumor shrinkage in grade 2 lesions, with modeling suggesting a threshold of ~135 Gy for high tumor control probability. At the patient level, mean tumor AD across the entire tumor burden was an independent predictor of progression-free and overall survival. Patients receiving cumulative tumor AD >118 Gy had significantly improved outcomes without increased toxicity.

These findings support the feasibility and safety of dosimetry-guided PRRT and strengthen the evidence for a dose–response relationship in NET. While causality cannot be fully established due to biological confounders, the results provide a rationale for future trials evaluating individualized treatment schemes based on tumor dosimetry.

Keywords: neuroendocrine tumors, peptide receptor radionuclide therapy, dosimetry, absorbed dose, dose-response, survival, tumor response

Language: English/Swedish **Number of pages**: 68

ISSN and key title: 1652-8220

ISBN: 978-91-8021-801-6

Dose-response relationships in neuroendocrine tumors treated with peptide receptor radionuclide therapy

Carl Fredrik Warfvinge

LUND
UNIVERSITY

Cover image by Hanna Maria Warfvinge and Hedvig Warfvinge

Faculty of Medicine
Department of Clinical Sciences
Lund University
Lund 2025

ISBN 978-91-8021-801-6
ISSN 1652-8220
Series title: Faculty of Medicine Doctoral Dissertation Series 2026:3

Printed in Sweden by Media-Tryck, Lund University,
Lund, 2025

Dedicated to all patients and families affected by this disease

Table of Contents

List of Papers **8**
Thesis at a glance **9**
Abbreviations **10**
Background **11**
Neuroendocrine tumors 11
Radionuclide therapy 16
Internal dosimetry 18
Peptide receptor radionuclide therapy in NET 24
Aims **32**
Methods **33**
Data acquisition and material selection 33
Statistical considerations 36
Use of Generative AI 39
Results **40**
Paper I 40
Paper II 41
Paper III 42
Paper IV 44
Discussion **46**
Paper I 46
Paper II 47
Paper III 48
Paper IV 49
Future perspectives **51**
Populärvetenskaplig sammanfattning **53**
My contributions **56**
Acknowledgements **57**
References **58**

List of Papers

Paper I Sundlöv A, Sjögreen Gleisner K, Tennvall J, Ljungberg M, **Warfvinge, CF,** Holgersson K, Hallqvist A, Bernhardt P and Svensson, J. Phase II trial demonstrates the efficacy and safety of individualized, dosimetry-based ^{177}Lu-DOTATATE treatment of NET patients. Eur J Nucl Med Mol Imaging (2022)49:3830 3840. DOI: 10.1007/s00259-022-05786-w

Paper II Roth D, Gustafsson J, **Warfvinge CF**, Sundlöv A, Akesson A, Tennvall J, Sjögreen Gleisner K. Dosimetric Quantities in Neuroendocrine Tumors over Treatment Cycles with ^{177}Lu-DOTATATE. J Nucl Med. 2022;63(3):399-405. DOI: 10.2967/jnumed.121.262069

Paper III **Warfvinge CF**, Gustafsson J, Roth D, Tennvall J, Svensson J, Bernhardt P, Åkesson A, Wieslander E, Sundlöv A, Sjögreen Gleisner K. Relationship Between Absorbed Dose and Response in Neuroendocrine Tumors Treated with [^{177}Lu]Lu-DOTATATE. J Nucl Med. 2024;65(7):1070-5. DOI: 10.2967/jnumed.123.266991

Paper IV **Warfvinge CF**, Curkic Kapidzic S, Gustafsson J, Jessen L,Svensson J, Sundlöv A, Sjögreen Gleisner K. Patient survival and its relation to tumor absorbed dose in [^{177}Lu]Lu-DOTA-TATE therapy of neuroendocrine tumors. Manuscript

Thesis at a glance

Paper	Aims	Patients/Tumors and Methods	Findings
I	Assessing safety and efficacy of the ILUMINET study in which ^{177}Lu-DOTA-TATE treatment schemes were individualized through dosimetry.	97 patients with non-curable NET G1-G2 were included. A combination of planar scintigraphies and SPECT/CT were used for dosimetric assessments. Continous 7.4 GBq treatments were given until a cumulative renal BED of 28 or 40 Gy depending on risk factor for kidney toxicity.	No serious renal side effects were seen. ORR was 34 %, median PFS and OS 29 and 47 months, respectively.
II	Assessing the evolution of dosimetric parameters in NET tumors across treatment cycles	880 dosimetric assessments from 182 tumors from 42 patients from ILUMINET were included. Tumor activity concentration, absorbed-dose rate, effective half-time and AD were calculated and linear mixed models were used for analysis.	Activity concentration, absorbed dose rate and AD decrease over cycles, more so for G2 than G1 tumors
III	Assessing the association between tumor AD and tumor volume change for individual tumors.	69 tumors from 32 patients from ILUMINET were included. Individual tumor volumes were manually assessed in consecutive CT scans. Associations between individual tumor AD and tumor volume changed were assessed with mixed models and logistic regression.	Mean tumor AD differ significantly between responding and non-responding G2 tumors. 135 Gy is a proposed threshold for tumor response.
IV	Assessing the association between mean AD across the entire tumor burden and survival outcomes	96 patients from the ILUMINET study were included. Mean AD (mass-weighted) to the entire tumor burden was assessed using an automated method. Kaplan-meier, log rank and uni- and multivariable cox regression were used to assess survival differences between high and low AD groups.	A tumor AD above 74 Gy (median) is an independent predictor of PFS and OS. A threshold of 118 Gy tumor AD is proposed for maximum effect.

Abbreviations

AD	Absorbed dose
BED	Biologically equivalent dose
CI	Confidence interval
DCR	Disease control rate
GEP-NET	Gastroenteropancreatic neuroendocrine tumors
HR	Hazard ratio
HRQoL	Health related quality of life
LQ-model	Linear-quadrant model
NET	Neuroendocrine tumors
ORR	Overall response rate
OS	Overall survival
PET	Positron emission tomography
PFS	Progression free survival
pNET	Pancreatic neuroendocrine tumors
PRRT	Peptide receptor radionuclide therapy
PVE	Partial volume effect
ROC	Receiver operating characteristic
siNET	Small intestinal neuroendocrine tumors
SIRT	Selective internal radiation therapy
SPECT	Single-photon emission computed tomography
SSA	Somatostatin analog
SST	Somatostatin
SSTR	Somatostatin receptor
TCP	Tumor control probability
tMN	Therapy-related myeloid neoplasms
VOI	Volume of interest

Background

Neuroendocrine tumors

Symptoms and diagnosis

Neuroendocrine cells are specialized cells present in most human organs. In essence their purpose is to release hormones upon receiving an external stimulus. Pancreatic neuroendocrine cells, for example, release the blood-sugar regulating hormones glucagon and insulin upon detecting changes in blood sugar levels (1-3), and small intestinal neuroendocrine cells release the hormone serotonin that modulate gut function upon chemical, mechanical or neural stimulation (4, 5).

Neuroendocrine tumors (NET) are malignant, well-differentiated tumors expressing a certain set of biomarkers proving their origin in neuroendocrine cells (6). Contrary to most malignancies, NET can arise in virtually any organ, due to their mother-cells' presence in most human tissues. Most commonly they arise in the gastrointestinal tract (including its adjacent organs) and in the lungs. The clinical presentation of NET varies depending on the organ of origin, disease stage, and the presence of hormone overproduction. In general, though, gastroenteropancreatic neuroendocrine tumors (GEP-NETs) often present with gastrointestinal symptoms that have typically developed over a considerable amount of time. Indeed, the diagnosis of NET is a considerable clinical challenge and is often delayed. This is attributed to its characteristically slow onset, which lowers clinical suspicion of malignancy, combined with a symptom profile that often resembles more common conditions such as irritable bowel syndrome (7). In many cases, patients are asymptomatic even in the presence of metastases, as illustrated in a cohort from Rigshospitalet in Copenhagen. Here 23% of metastasized small intestinal NET (siNET) and 25% of of metastasized pancreatic NETs (pNETs) were diagnosed incidentally through unrelated imaging or procedures (8).

Advanced siNET are commonly associated with serotonin overproduction. This can lead to carcinoid syndrome, characterized by diarrhoea, flushing, and an increased risk of heart valve fibrosis. At the time of diagnosis, 56% of patients with advanced siNET present with carcinoid syndrome (9). Pancreatic NETs more rarely produce symptom-inducing hormones (mainly gastrin, insulin, or glucagon) but when they do, they frequently cause significant clinical manifestations (10).

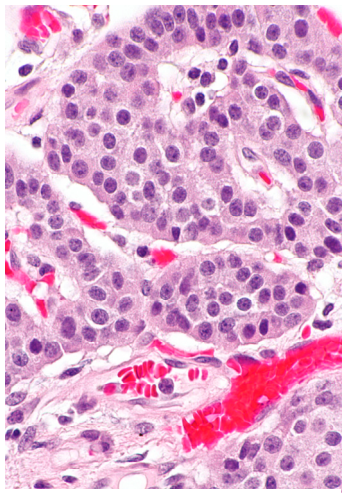

Figure 1. Histological section of a neuroendocrine tumor showing uniform round cells with finely granular cytoplasm and characteristic "salt-and-pepper" chromatin.

Pathological diagnosis of NETs relies on histological examination of tumor tissue, typically obtained through biopsy or surgical resection. The tumors are characterized by uniform, round cells with granular cytoplasm, "salt-and-pepper chromatin and a low mitotic index (11). Immunohistochemistry plays a central role in confirming the neuroendocrine origin, with markers such as chromogranin A, synaptophysin, and CD56 being commonly expressed (12), see example in Figure 1.

Classification and epidemiology

NET is a heterogeneous disease. Not only do different origin sites alter clinical presentation and prognosis, but so does the biological aggressiveness of the disease. Histopathological assessment of tumor aggressiveness is performed through the concept of tumor grade, with a higher grade indicating a more aggressive phenotype. According to the WHO classification (13), GEP-NETs are categorized into three grades (G1, G2 and G3) according to the rate of mitoses (numbers per 2 mm^2) and the percent of tumor cells expressing the proliferation marker Ki67. Lung NETs on the other hand are categorized into two categories G1 and G2 (also called typical and atypical carcinoids, respectively) according to rate of mitosis and the presence of necrosis (Table 1).

Table 1. Classification of GEPNET and lung NET. Ki-67 is not part of official lung NET classification; necrosis is not part of GEP-NET grading

Tumor type	Grade	Mitoses per 2 mm²	Ki-67 index	Necrosis
GEP-NET	G1	<2	<3%	Not required
	G2	2–20	3–20%	Not required
	G3	>20	>20%	Not required
Lung NET	Typical carcinoid (G1)	<2	Not required	Absent
	Atypical carcinoid (G2)	2–10	Not required	Focal necrosis

Tumor grade is a strong predictor of patient outcome. In cases diagnosed in the US between 2000 and 2012 (14), the hazard ratio (HR) for G2 versus G1 was 1.76 (95% confidence interval [CI] 1.59–1.94), adjusted for age, stage, and tumor origin. For G3 versus G1, the HR was 5.26 (95% CI 4.85–5.71). It should be noted, however, that this comparison also included poorly differentiated neoplasms, commonly

referred to as neuroendocrine carcinomas, which may artificially elevate the hazard ratio because these carcinomas have a substantially worse prognosis than well-differentiated G3 tumors.

According to the latest epidemiological report from the US (15), the total NET incidence in 2021 was 8.5 cases per 100,000 Americans. The incidence is heavily age-dependent with an estimated 17.6 cases (per 100,000) through ages 50-64 and 28.4 cases (per 100,000) for ages 64 and above. Moreover, incidence has risen steadily since the 1970s, probably due to a combination of improved diagnostics and an ageing population. Data from the Cancer Registry of Norway, encompassing all cases diagnosed between 1993 and 2021, showed that the prevalence of NET was 99.3 per 100.000 people. Notably, this includes patients with cured and non-cured disease (16).

At diagnosis, most patients have localized disease. However, a sizeable portion of patients - at least 19 % of cases diagnosed between 1970 and 2021 - had distant metastases at time of diagnoses. The presence of distant metastases dramatically worsens prognosis. For patients with localized disease, median overall survival is several decades, while it is 80 months for patients with distant metastases (15), who also suffer from impaired quality of life compared to the average population (17).

The somatostatin receptor

For both treatment and diagnosis of NET, the somatostatin receptor (SSTR) is essential. The somatostatin receptor is a family of G protein-coupled receptors that mediate the inhibitory effects of the peptide hormone somatostatin (SST) on hormone secretion and cell proliferation. Five subtypes are known amongst which SSTR subtype 2 is present in two variants, SSTR 2a and b (derived from the same gene, but through different RNA-slicing). All subtypes have high affinity for somatostatin (SST), a peptide hormone existing in two variants consisting of 14 (SST-14) or 28 (SST-28) amino acids, respectively.

When activated by somatostatin, these receptors trigger intracellular signalling pathways that suppress hormone secretion and cellular proliferation while promoting apoptosis (18). The binding of SST to the SSTR also induces the internalization of the receptor-ligand complex into the cytoplasm upon, a function important for radionuclide therapy. SSTR are expressed throughout several tissues (19), but is especially important for neuroendocrine cells. After malignant transformation into neuroendocrine tumors cells, SSTR expression is often retained, allowing the SSTR as a diagnostic and therapeutic target.

For diagnostic purposes, positron emission tomography (PET) using radiolabelled somatostatin analogs has become the gold standard for visualizing SSTR expressing tissues. The radiotracer consists of three elements: a radionuclide (e.g., ^{68}Ga), a

peptide capable of binding to SSTR, and a chelator (e.g., DOTA), which links the peptide and radionuclide, see Figure 2.

The most widely used radiotracers are ^{68}Ga-DOTA-TATE and ^{68}Ga-DOTA-TOC. "TOC" and "TATE" are commonly used short names that distinguish different structural variants of somatostatin analogs. Both binds with high affinity to SSTR subtype 2 (20), the predominant receptor subtype expressed in well-differentiated neuroendocrine tumors(19). Both ^{68}Ga-DOTA-TATE and ^{68}Ga-DOTA-TOC PET imaging provide high sensitivity and specificity for detecting primary and metastatic NET lesions (21). Likewise, SSTR can be used as a therapeutic target by leveraging its normal biological functions as an inhibitor of hormone secretion and cell proliferation and as an inducer of apoptosis. Long-acting SSTR agonists, called somatostatin analogs (SSA), activate these inhibitory pathways, leading to decreased hormone production and tumor growth.

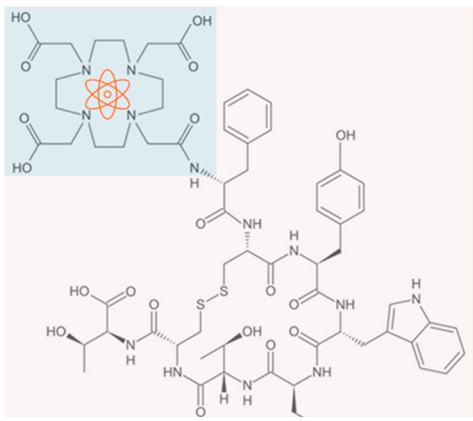

Figure 2. Molecular structure of DOTA-TATE. The somatostatin receptor agonist (TATE) is denoted in pink and the chelator (DOTA) in blue. The orange symbol represent the place of the radionuclide (e.g. ^{68}Ga).

Treatment of advanced NET

Given the heterogeneity of NETs, both in terms of stage at presentation, origin site, hormones production status and aggressiveness, treatment is highly circumstantial. In most cases, however, the only curative approach is to remove all tumor tissue through surgery. In cases with residual or metastatic disease this approach is generally not possible, and the aim of patient care is therefore to prolong and improve patient life as much as possible.

In essence, the overarching aim of sequence of therapies is to hinder disease progression and symptoms while exposing the patient for as little therapy related adverse effects as possible. Typically, patients with NET with a Ki67-index below 10 % start treatment with a long-acting somatostatin-analog (SSA), provided that ^{68}Ga-DOTA-TOC/TATE PET demonstrates that the tumor cells retain their SSTR expression. SSA is typically given once every 4 weeks and is administered by the primary care or by the patient themselves. While treated with SSA, patients can experience steatorrhea due to inhibition of SSTR-dependent inhibition of pancreatic juice production, gallstones due to SSTR-dependent inhibition of cholecystokinin production, and altered blood sugar levels (22), but in general clinical experience a majority of patients tolerate it well.

Upon disease progression, other, potentially more toxic pharmaceuticals are recommended. Table 2 summarizes the approved alternatives for advanced NET.

Table 2. Summary of the indications and key clinical trials for the approved treatments of advanced NET.

Drug	Class	Indication	Key Clinical Trial
Octreotide Long-Acting Release	Somatostatin analog	Symptom control and tumor growth inhibition in functional GEP-NET	PROMID (23)
Lanreotide	Somatostatin analog	Non-functioning GEP-NET	CLARINET (24)
Everolimus	mTOR inhibitor	Advanced lung and GEP-NET	RADIANT-3 and RADIANT-4 (25, 26)
Sunitinib	Tyrosine kinase inhibitor	Advanced pNETs	SU011248 (27)
Cabozantinib	Tyrosine kinase inhibitor	Previously treated advanced pNETs and extra-pancreatic NETs	CABINET (28)
^{177}Lu-DOTA-TATE	Peptide receptor radionuclide therapy	Advanced, progressive GEP-NETs	NETTER-1 (29)
Temozolomid+capecitabine	Chemotherapy	Advanced pNETs	ECOG-ACRIN E2211 (30)

Summary

NET is a fairly uncommon disease but with fatal and life-quality impairing consequences for many patients. This puts a moral obligation on the research community to try and improve patient care. The focus of this thesis is if and how dosimetry can be utilized to individualize treatment, with the goal of optimizing therapeutic efficacy while maintaining tolerable levels of adverse effects.

Radionuclide therapy

Discovery of radioactivity

On the afternoon of 20th January 1896, Henri Becquerel, professor of Applied Physics at *École Polytechnique*, attended a meeting of *l'Académie des sciences* in his native Paris. In attendance was polymath Henri Poincaré who lectured on a newly discovered form of radiation which a hitherto unknown German physicist named Wilhelm Röntgen had discovered a few months earlier, which produced distinct shadows of bones and dense objects on photographic plates (31). Röntgen had named this mysterious radiation X-rays. Inspired by his Teutonic colleague's work, Becquerel hypothesized that the fluorescent materials he used in his own research emitted X-radiation when exposed to sunlight. To this end, he exposed uranium salt (a known fluorescence) to sunlight and placed them near a photographic plate. After development, the contours of the salt crystals were readily visible on the photographs, supporting his hypothesis (32). Bad weather inhibited further experiments, and Becquerel instead let the crystals and the photographic plates rest close together in a cabinet. Upon development of these plates, he saw the contours of the crystals just as clearly as when they had been exposed to sunlight (33). Becquerel realized that the uranium salts emitted radiation spontaneously (34), a phenomenon that would later be named radioactivity. Ernest Rutherford soon classified the three types of radiation emitted from radioactive materials: alpha (α), beta (β), and gamma (γ), differing in particle type, mass, charge, and penetration depth. The different properties from these types of radiation are profoundly important in the field of nuclide medicine.

Early radionuclide therapy

Up until 1934, all known radioactive substances had been discovered as naturally occurring minerals in ores. However, during the 1930s, pioneered by Frederic Joliot and Irene Curie (daughter of Marie and Pierre), many artificial unstable isotopes were created by irradiating stable elements. By 1940, hundreds of such isotopes were known (35). These artificial isotopes had two distinct advantages for medical applications. Firstly, their half-lives were generally much shorter (ranging from hours to days) compared with naturally occurring radioactive materials. Secondly, artificial isotopes of elements normally present in the body are metabolized in the same way as their stable counterparts, allowing them to accumulate selectively in specific organs, such as iodine in the thyroid gland.

The first medically applied radioisotope was the β-emitter ^{32}P, administered at the University of California to seven patients with chronic leukemias and polycythemia vera. An activity of about 2 millicuries (74 MBq) was given in repeated doses. Notably, even at this early stage of radionuclide therapy, dosimetricS considerations

were explicitly made: based on calculated β-energy absorption, the estimated whole-body exposure was kept below 3 röntgen (36).

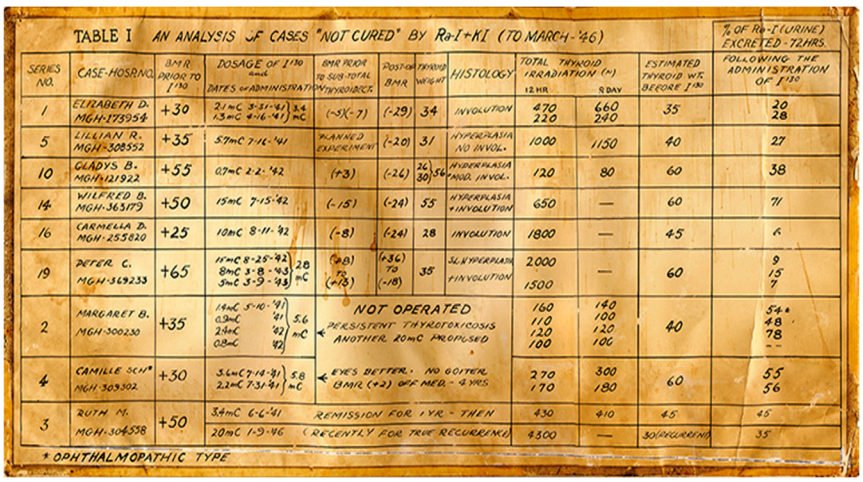

TABLE I AN ANALYSIS OF CASES "NOT CURED" BY Ra-I+KI (TO MARCH-'46)

SERIES NO.	CASE-HOSP.NO.	BMR PRIOR TO I^{130}	DOSAGE OF I^{130} mc & DATES OF ADMINISTRATION	BMR PRIOR TO SUB-TOTAL THYROIDECTOMY	POST-OP BMR	THYROID WEIGHT	HISTOLOGY	TOTAL THYROID IRRADIATION (+) 12 HR	TOTAL THYROID IRRADIATION (+) 5 DAY	ESTIMATED THYROID WT. BEFORE I^{130}	% OF Ra-I (URINE) EXCRETED - 72 HRS. FOLLOWING THE ADMINISTRATION OF I^{130}
1	ELIZABETH D. MGH-173954	+30	2.1mC 3-21-41 1.3mC 4-16-41	(-5)(-7)	(-29)	34	INVOLUTION	470 220	660 280	35	20 28
5	LILLIAN R. MGH-308352	+35	57mC 7-14-41	PLANNED EXPERIMENT	(-20)	31	HYPERPLASIA NO INVOL.	1000	1150	40	27
10	GLADYS B. MGH-121922	+55	0.7mC 2-2-42	(+3)	(-22)	26 30	56 HYPERPLASIA MOD. INVOL.	120	80	60	38
14	WILFRED B. MGH-365173	+50	15mC 7-15-42	(-15)	(-24)	55	HYPERPLASIA + INVOLUTION	650	—	60	71
16	CARMELLA D. MGH-255820	+25	10mC 8-11-42	(-8)	(-24)	28	INVOLUTION	1800	—	45	6
19	PETER C. MGH-369233	+65	11mC 8-25-42 8mC 3-8-43 5mC 3-9-43	(+8) TO (+13)	(+36) TO (-18)	35	28 mC SL. HYPERPLASIA + INVOLUTION	2000 1500	—	60	9 15 7
2	MARGARET B. MGH-300230	+35	1.4mC 5-10-41 0.9mC '41 2.4mC '42 0.8mC '42	5.6 mC	NOT OPERATED — PERSISTENT THYROTOXICOSIS ANOTHER 20mC PROPOSED			160 110 120 100	140 100 120 100	40	54* 48 78 --
4	CAMILLE SCH* MGH-309302	+30	3.4mC 7-14-41 2.2mC 7-31-41	5.8 mC	EYES BETTER. NO GOITER. BMR (+2) OFF MED. - 4 YRS.			270 170	300 180	60	55 56
3	RUTH M. MGH-304558	+50	3.4mC 6-6-41 20mC 1-9-46	REMISSION FOR 1 YR. - THEN (RECENTLY FOR TRUE RECURRENCE)				430 4300	410 —	45 30(RECURRENT)	45 35

* OPHTHALMOPATHIC TYPE

Figure 3. Dr. Saul Hertz's laboratory notebook. Of particular note is the efforts to quantify the absorbed dose, Printed with permission of Barbara Hertz, daughter of dr Saul Hertz.

In parallel, in Massachusetts, dr Saul Hertz started treating patients with hyperthyroidism with ^{130}Iodine and ^{131}Iodine with good results. Administration in patients were preceded by thorough studies of the uptake of radioactive iodine in rabbit thyroids, enabling estimation for reasonable activities to administer to patients (37). Most patients received administered activities of around 10-15 millicurie (370-525 MBq). He also indirectly estimated the total radiation to the thyroid (expressed in röntgen) through repeated measurement of the γ-radiation from the thyroid and integrating this over time (38), see Figure 3. In 1946, the first publication on radioiodine in metastatic thyroid carcinoma was published. Researchers first administered a tracer activity of radioiodine and monitored uptake in known metastases with a Geiger counter, to ensure iodine uptake. ^{130}I and ^{131}Iwere thereafter administered at repeated occasions with good effect on general symptoms and pain (39).

Absorbed dose

In the post-war period, the clinical use of radiotherapy, including radionuclide therapy, expanded substantially. This increasing application of ionizing radiation in medicine created a growing demand for precise dose planning and a standardized unit to express the impact of radiation on human tissue. The previously used unit for radiation exposure, the röntgen, proved insufficient, as it only quantified ionization in air. For therapeutic applications, the key parameter became the energy

deposited in tissue, which correlates with the ionizing potential and thus the biological effects - both therapeutic and harmful - of radiation. This led to the adoption of the concept of absorbed dose (AD), which remains the central quantity for assessing biological impact. Since 1975, the SI unit for absorbed dose has been the gray (Gy), defined as the absorption of one joule of energy per kilogram of matter (1 Gy = 1 J/kg) (37).

Invention of the gamma camera

The history of modern clinical radionuclide imaging started with an electrical engineer, Hal Anger, who worked at Berkeley in California in the 1950s and 1960s. He aimed to translate the invisible gamma radiation into images, a challenge that required a system capable of preserving spatial information and converting photon energy into a measurable signal. This was achieved through several integrated components: a collimator to restrict photon paths, a sodium iodide crystal to convert photon energy into light flashes, and photomultiplier tubes to transform these flashes into electrical pulses for imaging. Anger's original system was fully analog, using voltage signals to draw the image directly on film, but the same principle—though refined and digitalized—is still used in gamma-cameras today(40, 41). Building on this concept, a rotating version of the gamma camera was later developed, laying the foundation for single-photon emission computed tomography (SPECT) and enabling three-dimensional visualization of radiotracer distribution(37). A SPECT system is a gamma camera that detects gamma radiation from multiple angles around the patient and uses this data to reconstruct a 3D representation of the radiopharmaceutical distribution within the patients´ body.

Internal dosimetry

Overview

Dosimetry refers to the methods used to estimate the absorbed dose of ionizing radiation in matter. While highly relevant for all types of radiotherapy, here we will focus on the principles and techniques used to determine the absorbed dose from radiopharmaceuticals within the human body, commonly referred to as internal dosimetry.

A radionuclide is an unstable atom with excess energy. To reach a more stable state, it emits energy in the form of particles or electromagnetic radiation. Radionuclides used in medicine are typically artificially produced, most commonly by irradiating stable atoms in a nuclear reactor or a cyclotron. The type of emissions, as well as their energy and tissue penetration, vary between radionuclides. Table 3 summarizes the main types of emissions relevant to nuclear medicine.

Table 3. Comparison of Radiation Emission Types in Nuclear Medicine. *x_{90} represents the radius of a sphere within which 90% of the energy emitted is absorbed

Emission Type	Composition	Mean energy	Range	Example Medical Use
Alpha (α)[42]	2 protons + 2 neutrons	5 -9 MeV	50–100 µm	Therapy (e.g. ^{212}Pb, ^{225}Ac, ^{213}Bi)
Beta minus (β^-)[43]	Electron	0.1–0.9 MeV	0.5-5.5 mm (x_{90}*)	Therapy (e.g. ^{177}Lu, ^{90}Y, ^{131}I, ^{161}Tb)
Gamma (γ) [43] [44]	Electromagnetic photon	0.1-0.6	>1m	Imaging (e.g. ^{99m}Tc, ^{111}In, ^{123}I)
Auger electrons[43]	Electron (atomic origin)	<10 keV	<1 µm	DNA-targeted therapy (e.g. ^{111}In)

Each radionuclide has a unique nuclear structure and decay scheme, which determines the emission type and the energies of the emitted particles or photons. Consequently, radionuclides emitting the same type of radiation (e.g., β particles) produce emissions with different energies. These energies, in turn, govern both the penetration depth in tissue and the ionization density of the radiation, which are critical factors in both imaging and therapeutic applications.

For this thesis, we will focus on the imaging and therapeutic applications of ^{177}Lutetium. Lutetium is a chemical element classified as a *rare earth metal*, a group that includes several elements essential to both modern electronics and radionuclide therapy. Noteworthy, the term *rare earth* does not reflect actual scarcity of these elements in the Earth's crust. In fact, many of them, including lutetium, are relatively common. Rather, the term originates from a historical perception of them being rare(45). Most of the worlds lutetium (and other rare earth metals) is mined and purified in the far east (46) through complicated processes that have raised concern about local environmental impact (47).

^{177}Lutetium can be produced by neutron irradiation of targets made of ^{176}Lutetium or ^{176}Ytterbium, both virtually stable isotopes. In both cases, the target captures neutrons, forming either ^{177}Lutetium directly or ^{177}Ytterbium (another rare earth metal), which subsequently decays into ^{177}Lutetium. Because such processes require a high neutron flux, production cannot be carried out locally but must take place in the few specialized facilities worldwide with the necessary reactor capacity (48). The combination of mining, purification, and isotope production thus creates a supply chain that is both costly and vulnerable to disruption.

Upon decay, ^{177}Lu emits β^- particles (electrons) with mean and maximum energies of 147 keV and 498 keV, corresponding to a mean range in tissue of 0.3 mm (49). In parallel, two gamma-photons with energies of 113 keV and 208 keV, are emitted. The therapeutic effect of ^{177}Lu is derived from the electrons, while the two photons enable detection by a gamma camera.

To estimate the clinical impact of ^{177}Lu-based radionuclide therapy, one must first quantify the absorbed dose, i.e., the amount of energy deposited per unit mass of tissue. This is, as mentioned earlier, expressed in the unit Gy.

$$Absorbed\ dose\ (Gy) = \frac{Deposited\ energy\ (J)}{mass\ (kg)} \quad (1)$$

Quantification is achievable due to the emission characteristics of ^{177}Lu, where the number of emitted electrons is proportional to the number of detectable photons.

Quantification of activity and volume

A gamma camera can be used to measure the photon counts originating from ^{177}Lu decays occurring within a defined volume over a specified time interval. If the rate of radioactive decay (the activity) that gives rise to these counts can be quantified, it is possible to calculate the number of electrons emitted per unit of time and the energy emission within the same volume during that time interval. Thus, accurate quantifications of both activity and volume are central.

Determining a volume requires a three-dimensional representation, which can be obtained from anatomical imaging such as CT or MRI, or from functional imaging modalities like SPECT or PET/CT.

To accurately quantify the activity in a patient, several factors must be controlled. When determining the ^{177}Lu activity in a specific region (for example a tumor) it is crucial that the counts recorded by the gamma camera originate from photons emitted in that region, and that these counts can be reliably related to the underlying number of decays. A key concept in this context is the energy spectrum of the photons. Photons emitted by ^{177}Lu, primarily with energies 113 keV and 208 keV, traverse the body. During the journey, they may interact with atoms in other tissues, causing the photons to lose energy and/or change direction, processes known as photon scattering and attenuation. Scattering can be mitigated by applying energy windows that discard photons outside predefined energy ranges and by using collimators to filter out photons entering the gamma camera at oblique angles. The degree of photon interaction depends on the types of tissues the photons pass through on their journey from the site of radioactive decay to the camera. Denser tissues give a higher probability of photon interaction. Consequently, more photons are detected when passing through less dense organs (e.g., lungs), whereas fewer are detected when the photons pass through denser structures such as bone. To compensate for this, information from an x-ray scout or CT scan is used to estimate the interaction properties of the tissues.

Gamma-camera imaging can be made with planar scans or SPECT imaging, yielding two- and three-dimensional images, respectively. Planar images have the advantage of whole-body coverage but suffer from the superposition of activity

along the anterior-posterior direction, which makes accurate activity quantification difficult, as displayed in Figure 4.

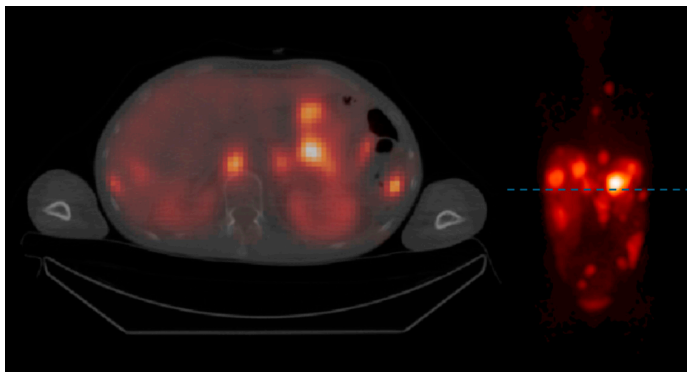

Figure 4. Left image shows a transversal SPECT/CT plane with tumors and the left kidney indicated by white arrows. Right image shows planar image of the same patient, acquired at the same occasion (nominally 24 h post administration). In the SPECT image, ^{177}Lu activities in tumors and kidneys are resolved in the anterio-posterior direction, whereas they are superimposed in the planar image.

SPECT images are obtained from tomographic reconstruction of a set of planar images (projections) acquired when the gamma camera rotates around the patient. The tomographic reconstruction embeds corrections for attenuation and scattering and is performed by iterative methods. During these iterations, the measured numerical values in the planar images are compared with those representing the current reconstructed image, and any discrepancies compensated for. The more iterations, the higher the spatial and quantitative accuracy, but at the cost of increased image noise and longer computation time.

The gamma camera and reconstructed SPECT image have characteristic spatial resolutions, typically measured in millimeters. The spatial resolution describes the ability to distinguish between two separate radioactive sources; the better the resolution, the smaller the distance between two imaged radiation foci. In nuclear medicine images, the limited spatial resolution is manifested as a blurring of the imaged object. For SPECT, the reconstruction method can compensate for some of the blurring, employing so-called resolution recovery methods.

The limited spatial resolution introduces a potential source of error known as the *partial volume effect* (PVE). The partial volume effect reflects the camera's inability to accurately quantify activity in small structures due to signal blurring and spill-out. The concept is illustrated in Figure 5.

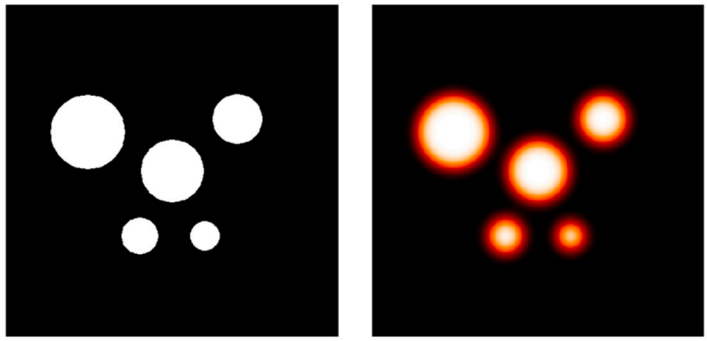

Figure 5. Circular objects (left) corresponding to cross-sections of spherical sources of different diameters, all having identical activity concentrations. In the image (right), limited spatial resolution produces a blurred appearance with spill-out of counts from the object, and an object intensity that appears to be lower for the smaller objects. The partial-volume effect refers to this falsely low object intensity, which becomes gradually more severe for smaller object.

The larger the studied object, the smaller the relative impact of the PVE. To estimate the magnitude of this effect for a given volume, a parameter called the *recovery coefficient* is used. The recovery coefficient is defined as the ratio of measured activity concentration from a SPECT image to the activity concentration in a real object and is used to correct for the error introduced by the PVE across different object volumes.

From activity concentration to absorbed dose

For next step towards determining the absorbed dose, we must use the activity concentration to estimate the absorbed dose rate, i.e. the absorbed dose per second. To make this intuitive, let us look at the expressions:

$$\text{Activity concentration (Bq/ml)}\ \frac{\text{decays}}{\text{s} \times \text{ml}} \qquad \text{Absorbed dose rate (Gy/s)}\ \frac{\text{Joule}}{\text{s} \times \text{kg}}$$

From here, it is evident that we must convert volume to mass and activity (decays / s) to the rate of energy deposition in matter. Volume to mass is down to the density, which to a first approximation can be assumed to water, or can otherwise be estimated from a CT image of the patient. Converting activity to energy deposition involves considerably more steps.

In principle, the biological impact of the radionuclide is not localized at the site of decay, but along the entire path travelled by the emitted particles, which in the case of ^{177}Lutetium is electrons. In other words, the biological effect may extend from the point of decay, with the extent depending on the characteristics of the decay and the penetration length. For a radionuclide such as ^{90}Y that emits electrons with a

higher energy and a longer range, this penetration length may need to be considered in internal dosimetry. Fortunately, for our purposes, the electrons emitted by ^{177}Lu have a shorter range in soft tissue than the spatial resolution of the gamma camera and SPECT system. Therefore, it is a reasonable assumption that photon emissions and the biological effect of the electrons occur in approximately the same location. Thus, the photon-emitting volume can be considered equal to the volume of biological effect.

The last step in determining the absorbed dose is to integrate the absorbed dose rate over time. Importantly, the absorbed dose rate from ^{177}Lu diminishes over time. This comes down to two factors. Firstly, ^{177}Lu has a physical half-life of 6.6 days. Secondly, there is a biological half-time, depending on losses through physiological elimination processes such as faeces, urine and perspiration, but also the uptake and turnover of the radiopharmaceutical in the respective organ.

Thus, accurate estimation of the absorbed dose delivered to an organ or tumor requires either repeated activity quantifications or prior knowledge of the combined biological and radioactive half-lives.

Radiobiological impact

The radiobiological effect of the electrons emitted from ^{177}Lu is mainly through DNA damage. The DNA is damaged either directly, via ionization of atoms in the molecule, or, more commonly, via radiolysis of water to form reactive oxygen species, which subsequently interact with and damage the DNA (50). The human genome is continuously monitored by specialized proteins that detect damage and initiate repair cascades. Depending on the extent of the damage and the availability of repair mechanisms, the outcome may be complete restoration, cell cycle arrest, or impaired cellular function.

Generally, the time pattern with which an absorbed dose is delivered to tissue adds another layer of complexity to radiobiological effects. Because different tissues vary in their ability to repair radiation-induced damage, they respond differently to fractionation (the separation of the total activity administered into fractions). For example, in tissues with impaired cellular repair mechanisms, delivering a total absorbed dose in smaller fractions may result in significant damage, whereas tissues with proficient repair capacity may exhibit recovery between fractions.

The theoretical framework used to describe a tissue's relative sensitivity to increasing fraction doses is the linear-quadratic (LQ) model. It suggests that the surviving fraction of cells following radiation exposure depends on both a linear and a quadratic relationship, as:

$$\text{Surviving fraction of cells after radiation} = e^{-(\alpha D+\beta D^2)} \quad (2)$$

In Equation 2, α and β are tissue- and endpoint-dependent radiobiological parameters, and D is the total absorbed dose delivered. The parameter α is the constant representing the contribution of the linear component, while β represents the quadratic component. The higher the ratio between α and β, the larger the relative impact of the linear component. The BED (Biologically Effective Dose) is a way to compare different fractionation schemes by accounting for tissue-specific radiosensitivity. It normalizes the total absorbed dose using the α/β ratio, which reflects how sensitive a tissue is to changes in dose per fraction. Tissues with a low α/β ratio (e.g., late-responding normal tissues) are more affected by fraction size, while those with a high α/β ratio (e.g., tumors) are less sensitive. BED therefore provides a standardization of the absorbed doses required to cause a given biological effect across different fractionation schedules. The formula for BED is algebraically derived from an extended version of Equation 2 (51).

$$\text{BED} = D\left(1 + \frac{G \cdot D}{\alpha/\beta}\right) \qquad (3)$$

The tissue-specific and time-dependent factor, G, is introduced in this equation to take into account the increasing possibility of repair as the absorbed dose rate decreases (52). In external beam radiotherapy, the factor G is set to 1 and is often not included in the equation. For radionuclide therapy however, G will be less than 1 and is an important determinant of the BED. It is worth noting that the complexities of how to assess the BED of radionuclides is still insufficiently understood, with the European Association of Nuclear Medicine recently calling out for further research (53).

Before leaving the LQ-model, an important disclaimer must be expressed. While this half-century old mechanistic explanation is palatable and intuitive, the actual factors determining the dose-response in tissues in infinitely more complex. The LQ model must therefore be interpreted as an effective tool in preclinical and clinical radiobiology, rather than a singular, all-encompassing radiobiological model (54).

Peptide receptor radionuclide therapy in NET

Development of PRRT in NET

During a conference in Rotterdam in 1985, a paper was presented, discussing how SSTRs in NET were identified by labelling a somatostatin analog with ^{125}I (55). In attendance was the head of nuclear medicine at Erasmus MC in Rotterdam, Eric Krenning, who worked with ^{123}I and ^{131}I for imaging and treatment of thyroid cancer. The results presented at the conference strongly influenced Krenning, inspiring him to pursue the development of radiopharmaceuticals targeting SSTR-positive malignancies for clinical use (55).

The first clinically used radionuclide-SSA-complex was ^{111}In-DTPA-octreotide developed in the early 1990s (56). Upon decay, ^{111}In emits two gamma photons with characteristic energies, making it a suitable radionuclide for gamma camera imaging. In addition, ^{111}In emits Auger electrons with short range and high linear energy transfer (57), suggesting potential for therapeutic application. ^{111}In-DTPA-octreotide was initially used as a diagnostic agent and was approved for use by the Food and Drug Administration (FDA) in 1994. Octreoscan (as the compound was marketed) was a diagnostic tool until it was superseded by modern PET-methods in the 2010s.

The therapeutic potential of ^{111}In-DTPA-octreotide was also explored, by increasing the administered activity. Although disease stabilization and partial responses were observed, it was hypothesized that the short-range Auger electrons were therapeutically suboptimal and that treatment efficacy could be improved by replacing 111In with a β-emitter with greater tissue penetration. This, however, required a chelator-SSTR-complex capable of maintaining the β -emitter such that it did not dissociate in the blood stream with the risk of unacceptable side effects. This challenge was overcome in the late 1990s with the synthesis of DOTA-TOC (58). DOTA is a radiometal chelator possessing high thermodynamic and kinetic stability under physiological conditions (59) making it ideal for carrying potent therapeutic radionuclides.

^{90}Y-DOTA-TOC was the first beta-emitting radionuclide used for patients with NET. ^{90}Y emits high-energy beta particles with a tissue range of several millimeters, theoretically well-suited for treating bulky tumors. Clinical trials confirmed an improved tumor effect compared to Indium-based therapy(60, 61) (62). However, the same physical property that enhanced tumor penetration also increased radiation exposure to kidneys, the critical organ at risk. Renal toxicity, including cases requiring dialysis, was reported (62). Subsequent studies implemented renal-protective infusions to reduce severe toxicity, but the long-term risk of renal impairment remained a concern.

In the early 2000s, arguments were emerging for the use of ^{177}Lu (specifically via the chelator-somatostatin analogue complex DOTA-TATE) in PRRT (65). ^{177}Lu emits electrons with a shorter tissue range than ^{90}Y, potentially reducing collateral damage while maintaining therapeutic effect. Moreover, its γ-emissions facilitate post-therapy imaging and dosimetry, enabling treatment monitoring. 177Lu-DOTA-TATE was used in clinical studies including the Rotterdam cohort (64), and demonstrated favorable safety and efficacy, with low rates of severe renal toxicity and hematologic complications. Notably, it was given with renal protective amino acids. Initially, PRRT was not approved, but offered at specialized centers, often serving both domestic and international patients. For instance, large cohorts were treated in Milan, Rotterdam, Basel and Bad Berka (Germany). It was designated status as orphan drug by the European Medicines Agency in 2008 (66).

Table 4. A selection of pioneering studies on PRRT. SD = Stable disease, PR = Partial Response, ORR = Overall response rate, CR = Complete response. AA = Amino acid.

Radionuclide & ligand	Study / Reference	Patient group	Administered activity	Response	Toxicity
^{111}In-DTPA-octreotide	Valkema et al. (2002) (63)	40 NET patients	8–12 cycles, 6–7 GBq/cycle	53% SD/PR	Low renal tox, 3 hematological malignancies
^{90}Y-DOTA-TOC	Otte et al. (1999) (62)	29 NET patients	4+ cycles, 1.5–2.3 GBq/cycle	26 SD/PR, 3 PD	High renal tox without AA protection
^{90}Y-DOTA-TOC	Waldherr et al. (2001) (60)	41 NET patients	4 cycles, 0.9–2.0 GBq/m²	85% SD/PR	Mild hematological tox
^{90}Y-DOTA-TOC	Paganelli et al. (2001) (61)	30 NET patients	3 cycles, 1.11–2.59 GBq	23% ORR, 64% SD	Minimal renal tox
^{177}Lu-DOTA-TATE	Kwekkeboom et al. (2008) (64)	504 NET patients	4 cycles, 7.4 GBq	2% CR, 28% PR	Low renal tox, few MDS
^{177}Lu-DOTA-TATE	NETTER-1 (2017) [28]	Midgut NET	4 cycles, 7.4 GBq	PFS 65% at 20 months	No significant tox

The current approval of PRRT is based on the NETTER-1 study, a two armed, randomized, multi-center study comparing 4 cycles of 7.4 GBq ^{177}Lu-DOTA-TATE with high-dose SSA in patients with siNETs with disease progression on standard dose SSA alone. At the time of the first publication of the study in 2017, the estimated 20-month progression-free survival (PFS) rate was 65.2% (95% CI, 50.0 to 76.8) in the ^{177}Lu-DOTA-TATE -group, compared to 10.8% (95% CI, 3.5 to 23.0) in the control group (29), albeit no significant difference in median overall survival was detected at long term follow-up (67). Hitherto, Luthatera® is approved for SSTR-positive GEP-NET G1 and G2 in the European Union(68) and for SSTR-positive GEP-NET in the United States(69). Recommended treatment schedule is 7.4 GBq with 8 weeks intervals. Renal protective amino acids shall be administered in adjunction to the treatment.

Renal side effects of PRRT

Radiolabelled peptides are small molecules. In the kidneys, they pass readily through the glomerular filter into the proximal tubule. Here, a sizeable proportion are reabsorbed, contributing to a relatively high retention of the radionuclides the kidney (70). Radiation-induced kidney injury typically manifests long after exposure (71), limiting the utility of renal biomarkers for guiding treatment during therapy. To mitigate renal uptake, amino acids are co-infused with the radiopharmaceutical, competing for proximal tubular reabsorption and thereby markedly reducing kidney retention and absorbed dose (72).

^{90}Yttrium

The first report of kidney toxicity in PRRT patients treated with ^{90}Y-DOTA-TOC showed that 4 of 14 patients without renal-protective amino acids developed grade ≥3 renal adverse events, including 2 requiring hemodialysis, whereas none of the 15 patients receiving amino acids experienced severe renal toxicity (62). In Rotterdam, 28 patients were treated with ^{90}Y-DOTA-TOC and renal protective amino acids in a dose escalation study (64). Renal function declined progressively, with a median annual decrease in creatinine clearance of 7.3% among treated patients. In two patients, it was estimated that they would require dialysis in the future. They had received a total administered activity of 11.6 GBq and 22.9 GBq, respectively, corresponding to estimated renal absorbed dose of 27.5 and 27.0 Gy. A biopsy showing thrombotic microangiopathy, consistent with radiation induced damage was performed.

Later, a retrospective analysis from Basel with 1,109 patients receiving ^{90}Y-DOTATOC in various treatment schemes showed severe renal toxicity in 102 (9.8 %) patients. However, no difference in survival was seen in patients with and without severe renal toxicity (73). On the other hand, a retrospective analysis from patients treated in Bad Berka in Germany showed grade ≥3 renal side effect in 1 of 169 patients treated with ^{90}Y-PRRT alone and in 1 of 567 patients treated with ^{177}Lu-PRRT and ^{90}Y-PRRT in tandem(74). Similarly, among patients treated with ^{90}Y-PRRT in Milan, 5 out of 200 patients (2.5 %) showed grade ≥3 renal adverse events(75).

^{177}Lutetium

For ^{177}Lu-PRRT there have been fewer observations of renal impairment. In 407 patients treated in Rotterdam with ^{177}Lu-DOTA-TATE administered as 7.4 GBq x 4, or to an estimated kidney absorbed dose of 23 Gy, no treatment-related renal grade ≥3 adverse effects were seen on long follow up (76).

In the Bad Berka cohort, with 509 patients treated with 177-Lu-PRRT only a handful patients suffered from renal grade ≥3 adverse events and their conclusion was that Lu-PRRT was safe (74). In the Milan cohort, no renal grade ≥3 adverse events were reported among 278 patients treated with median administered activities of 22.9 GBq (75).

Data from the Basel cohort forms an outlier. Here, 13 out of 141 patients (9.2%) treated with ^{177}Lu-DOTA-TOC suffered from renal grade ≥3 adverse events. However, ^{177}Lu was the preferred radionuclide for patients with elevated creatinine levels (>90 μmol/L), which may limit the generalizability of these results.

Although renal toxicity appears to be rare with ^{177}Lu-PRRT, data from another radiopharmaceutical may serve as a reminder of its potential for inducing renal damage. A German group recently reported that the prevalence of grade ≥3 chronic kidney disease increased from 20% to 37% after administration of 7.4 GBq ^{177}Lu-

PSMA-I&T given in 4 cycles or more, for the treatment of metastatic prostate cancer (77). Biopsies from three patients showed thrombotic microangiopathy, consistent with radiation-induced kidney damage (78). Importantly, treatment schemes do not include renal-protective amino agents.

Improvement of PRRT

While PRRT has become a staple in the treatment arsenal of GEP-NETs, several interesting approaches to improve treatment further are being evaluated. This can broadly be divided into four categories: 1) Altering the carrier molecule, 2) Using other radionuclides 3) Combination therapies and 4) Adjusting treatment schemes through dosimetry.

Throughout the history of PRRT, somatostatin receptor agonists have been used, which bind to and activate SSTRs, leading to receptor internalization and intracellular trapping of the radioligand. Recently, **somatostatin receptor antagonists** have been evaluated in clinical settings. Unlike agonists, these bind to somatostatin receptors without triggering activation or internalization. Antagonists have been shown to have a higher tumor uptake and improved imaging contrast, because they recognize a broader range of receptor conformations and binding sites (79). A German group evaluated the somatostatin receptor antagonist LM3 as a carrier peptide for ^{177}Lu as ^{177}Lu-DOTA-LM3 (80). It was given to patients with G1-G3 tumors, where 69 % were pretreated with ^{177}Lu-PRRT. Disease control rate (DCR) at evaluation 3-6 months after treatment was 85.1 %. without severe hematological or renal side effects.

Another way of altering the carrier molecule is to add **Evans Blue.** Evans Blue binds reversibly to serum albumin, prolonging circulation time and improving tumor uptake. This allows for administering a lower activity per cycle while maintaining efficacy. A Chinese group evaluated the Evans Blue–modified agonist ^{177}Lu-DOTA-EB-TATE (81). in patients with metastatic NET. Treatment was generally well tolerated, with only a small proportion experiencing significant blood-related side effects. Disease control rate at 3–6 months was 85.2 and median PFS was 36 months.

Perhaps the most promising approach is to treat patients with an **α-emitter** rather than a β-emitter. α-particles have a significantly higher linear energy transfer than β-particles, resulting in dense ionization tracks that cause complex cell damage, making them a potent potential anticancer agent. Table 5 summarizes some of the studies conducted on α-emitters.

Table 5. Selection of studies on α-emitters in NET.

Author	Radiopharmaceutical	Diagnosis	Efficacy	Administered activiy	Toxicity
Ballal[82]	225Ac-DOTATOC	GEP-NET (G1-G3)	24 months OS prob 70.8%	100-120 kBq/kg every 8 week	Mild
Michler[83]	212Pb-VMT-α-NET*	GEP-NET (G1-G3)	100 % DCR 3 months post t	1.2 MBq/kg, single treatment	Mild
Delpassand[84]	212Pb-DOTAMTATE	Lung and GEP-NET (G1-G3)	Full dose 14 mo duration of response	Dose escalation to 2.50 MBq/kg x 4	Mild
Kratochwil[85]	213Bi-DOTATOC (intra-arterial)	Lung and GEP-NET (G1-G3)	No progression at time of analysis	6-11 GBq	Some renal toxicity. One case of AML.

Another pathway to improvement of PRRT is through **combination therapy** with other drugs. Chemotherapy (primarily temozolomide and/or capecitabine) has been explored in several studies. For example, Claringbold et al. (86) treated 30 patients with G1 and G2 pNET using four cycles of combined ^{177}Lu-DOTA-TATE à 7.9 GBq with concomitant temozolomide and capecitabine. This regimen resulted in an impressive median PFS of 48 months and ORR of 80%. One case of MDS was reported following treatment, but no renal toxicity or other serious hematological adverse events were observed. Although several prospective multi-arm studies have been initiated (87), none have yet been published. Therefore, a definitive assessment of the risk-benefit profile must await the results of these ongoing trials.

PARP-inhibitors, is another class of drugs that are being investigated in combination with PRRT. Preclinical studies have shown that PRRT combined with the PARP-inhibitor olaparib resulted in an increased number of double DNA strand breaks and cell death (88). A phase-I study from Gothenburg showed that olaparib 200 mg in combination with ^{177}Lu-DOTA-TATE was well tolerated (albeit associated with thrombocytopenia) in a cohort of G2 and G3 GEP-NET and lung NET (89).

Improvement of PRRT through dosimetry

Dosimetry-guided radiopharmaceutical treatment of cancers has proven safe and effective in several malignancies including papillary thyroid cancer and follicular lymphoma(90, 91). ^{177}Lutetium-PRRT dosimetry-guided studies have been conducted in Uppsala (92), where the number of treatment cycles were guided by the total absorbed dose to the kidneys (maximum 23 Gy) and bone marrow (maximum 2 Gy) and in Québec where the amount of administered activity was

guided by kidney dosimetry up to a limit of 23 Gy(93). In both these studies, renal toxicity was low. However, the proposed renal absorbed dose limit of 23 Gy is probably overly cautious. Originally it was derived from external beam radiotherapy and does not take the specific radiobiological mechanisms of radionuclide therapy into consideration (94).

When instead using BED as a metric, renal toxicity has typically not been observed below 28 Gy BED in patients with risk factors for kidney disease, and below 40 Gy BED in patients without such risk factors (95). This suggests that there may be room for increasing the renal absorbed dose limit, potentially improving therapeutic benefit without increasing toxicity.

However, if treatment schemes for PRRT are to be optimally guided by individual dosimetry, it is essential to assess not only the absorbed dose to organs at risk, but also whether tumors receive an adequate therapeutic dose. This dual focus mirrors the approach adopted in external beam radiation therapy, where detailed planning is performed to achieve target coverage while respecting organ-at-risk limits. Such knowledge could prevent unnecessary additional cycles when the required tumor absorbed dose has already been achieved, and conversely, support continued treatment beyond conventional risk-organ absorbed dose limits when tumor doses remain insufficient. A deeper understanding of this relationship between tumor absorbed dose and clinical benefit is therefore critical for optimizing treatment strategies.

A few studies have explored a dose-response relationship between tumor absorbed dose and clinical response. During the therapeutic attempts with 111In-PRRT, it was noted that 9 of the 10 patients with the highest visual tumor uptake grade on scintigraphy exhibited treatment effect (63). In a study from 2004, approximately 30 tumors from 13 patients treated with ^{90}Y-DOTATOC were assessed. Tumor absorbed dose was calculated from pretherapeutic 86Y-DOTA-TOC-PET, and tumor volume change was assessed by comparing CT volumes before and after treatment. Of special note, the median cumulative absorbed dose of responding tumors (232 Gy) was more than 6 times higher than the mean of non-responding tumors (37 Gy) (96).

In Uppsala, it has been shown that volume reduction for pNET and siNET (97, 98) is associated with a higher cumulative AD for individual tumors. Hebert et al. (99) reported a positive association between cumulative tumor absorbed dose and tumor shrinkage from baseline until 3 months post last treatment. Shrinkage was evaluated with CT, and the population encompassed 146 tumors from 35 patients, mostly G1 and G2 NET. However, the strength of the association was not reported. No tumors that progressed (defined as $\geq$ 20% volume increase) had received a cumulative absorbed dose above 95 Gy. Furthermore, among tumors with cumulative absorbed doses exceeding 95 Gy, additional shrinkage was not observed, indicating a saturation point in the dose–response relationship. Regarding tumor absorbed dose

and patient survival, Hebert et al reported that higher cumulative tumor absorbed doses were associated with improved PFS, with patients receiving higher than approximately 91 Gy across all lesions showing significantly longer PFS compared to those below this threshold, while a minimum lesion dose above 52 Gy was linked to both improved PFS and OS.

Mileva et al. (100) reported from a cohort of 35 patients. Patients whose selected target lesions all received at least 35 Gy during the first cycle had markedly longer PFS compared to those below this threshold (P=0.02; HR, 0.37; 95% CI, 0.17–0.82). Maccauro et al.(101) reported from a cohort of 42 patients. Patients with a mass-weighted mean tumor absorbed dose after the first cycle below 10.6 Gy had significantly shorter progression-free survival compared to those below this threshold (p = 0.004; HR, 8.6; 95% CI, 2.0–37).

While these studies support a positive relationship between tumor absorbed dose and clinical outcomes, important knowledge gaps remain. No study yet have reported fully adjusted multivariable survival analyses, and all of these studies are limited by modest sample sizes and, in some cases, relatively short follow-up periods. Thus, studies with larger cohorts and comprehensive multivariable modelling are needed to clarify the nature of this relationship and guide the development of personalized PRRT strategies.

Aims

"If you see a good move, look for a better one"

Pedro Damião, Portuguese chess author (1480-1544)

The overarching aim of this thesis has been to investigate the safety and effectiveness of dosimetry-guided PRRT in NET and to further our understanding of how tumor absorbed doses influence tumor behavior and clinical outcomes.

Specifically, the aims of the individual papers were:

Paper I To determine whether altering the number of PRRT cycles through renal dosimetry is safe and effective.

Paper II To understand how dosimetric quantities vary within and between patients, and throughout of the course of treatment, with consequences for the possibilities of simplifying dosimetry and to inform future treatment protocols.

Paper III To determine how absorbed dose to individual tumors influence tumor volume changes and to suggest a benchmark absorbed dose for tumor response.

Paper IV To determine whether mean tumor absorbed dose to the entire tumor burden predicts patient survival and to suggest a benchmark mean tumor absorbed dose for increased survival.

Methods

Data acquisition and material selection

Paper I

The ILUMINET Trial

The ILUMINET trial was a prospective phase II study conducted between 2011 and 2019 at two tertiary hospitals (Lund and Gothenburg) in Sweden. The trial aimed to assess the safety and efficacy of dosimetry-guided, individualized treatment of G1-G2 NET with ^{177}Lu-DOTA-TATE. Participants included in the study were adults with histologically confirmed progressive metastatic neuroendocrine tumors. Patients had to have tumors with Ki67 index of 20% or less, based on data suggesting a high degree of early progression rate for patients with G3 NET (102). Tumor lesions had to be measurable according to RECIST version 1.1 (103), and demonstrate somatostatin receptor uptake greater than that of normal liver parenchyma on scintigraphy. Individuals had to present with WHO performance status of 2 or lower, along with preserved liver and bone marrow function. Renal function was assessed prior to inclusion, requiring a baseline glomerular filtration rate of at least 50 mL/min/1.73 m^2, determined using either iohexol- or ^{51}Cr-EDTA clearance.

Patients received cycles of 7.4 GBq with 8–10-week intervals. Dosimetry was performed for each cycle to determine the renal BED. It was decided that altering the cumulative administered activity through changing the number of cycles rather than the administered activity per cycle was the safer option due to the low *a/b* of kidney tissue (104). The maximum tolerable kidney BED was derived from earlier studies on ^{90}Y-DOTA-TOC (95) indicating that patients with risk factors for renal failure (hypertension, age over 70, diabetes, previous trans-arterial chemo-embolization or platinum-derived chemotherapy) risked renal adverse event at a total renal BED of 28 Gy, while patients without these risk factors could tolerate an accumulated renal BED of 40 Gy. Treatment up to a total renal BED of 27 ± 2 Gy and 40 ± 2 Gy were called *Step 1* and *Step 2,* respectively. Amino-acid solution for renal protection was administered at each treatment.

Patients were followed with CECT (contrast-enhanced CT) or MRI until progression. Intervals between imaging were initially 3 months but could be extended up to 12 months in cases of stable disease.

Dosimetry

A dosimetric protocol to determine kidney absorbed doses had been developed and evaluated prior to the start of the study(105). The dosimetry method combined whole-body biplanar scintigraphy at 1-2, 24-, 48- or 96-, and 168-hours post infusion, with a SPECT/CT acquisition at 24 hours. An X-ray scout was performed at 1-2 hours for attenuation correction for the whole-body scans.

The effective half-life of the kidneys was determined from the planar images, while the SPECT was used to quantify the kidney activity at 24 hours. This information was combined and integrated over time to determine the kidney absorbed dose. As in earlier publication on BED in radionuclide therapy, an α/β ratio of 2.6 Gy and a repair half-time (a key determinant of the G factor, see Eq. 2) of 2.8 hours were assumed (81). These values were originally from an animal model (106).

Paper II

Material was derived from the subset of patients treated in Lund in the ILUMINET trial. Candidate tumors were manually identified on planar images and delineated into volumes of interest (VOI) semi-automatically according to an already published method (107, 108). Diagnostic images were inspected to verify that the VOIs indeed were tumors. Since the calculation of effective half-lives, and consequently absorbed dose, relied on planar imaging, tumors that overlapped antero-posteriorly in the planar views, as well as those located anterior to the kidneys or spleen, were excluded from the analysis. These tumors were however included in the analyses of absorbed dose rate and activity concentration, for which only the SPECT image was needed for quantification. Given that partial volume effect increases with decreasing VOI size, a tumor size cut-off at 8 cm^3 was adopted, based on a previous publication (108).

Paper III

Material was derived from the subset of patients treated in Lund in the ILUMINET trial. Dosimetric data were acquired as in Paper II. Tumors for which calculation of the cumulative absorbed dose was possible were assessed for inclusion. All post-baseline imaging studies, including contrast-enhanced CT and MRI, were reviewed to identify measurable tumors. Manual segmentation was performed using ARIA 15.6 (Varian Medical Systems, Inc.), and tumor boundaries were outlined accordingly, as illustrated in Figure 6. When multiple contrast phases were available, the phase offering the clearest and most consistent visualization across time points was selected. Lesions that could not be confidently distinguished, as well as those located in bone, were excluded from further evaluation. To avoid

confounding effects from tumors that were not susceptive to PRRT, lesions that progressed or led to patient death during the treatment period were excluded.

Once VOIs were defined, tumor volumes were automatically computed by the software and exported. These volumes were plotted against time since baseline to assess temporal changes visually. The largest and smallest volumes observed during follow-up were denoted as Vol_{max} and Vol_{min} respectively. The relative change in tumor volume was expressed in percent as:

$$\Delta Vol\% = \frac{Vol_{max} - Vol_{min}}{Vol_{max}} \times 100 \qquad (4)$$

The initial scan represented the maximum volume in the majority of cases. In some instances, the peak volume occurred at the first follow-up. Notably, for certain tumors, the minimum volume was reached prior to the final treatment cycle. For supplementary analysis, the smallest post-treatment volume was also recorded.

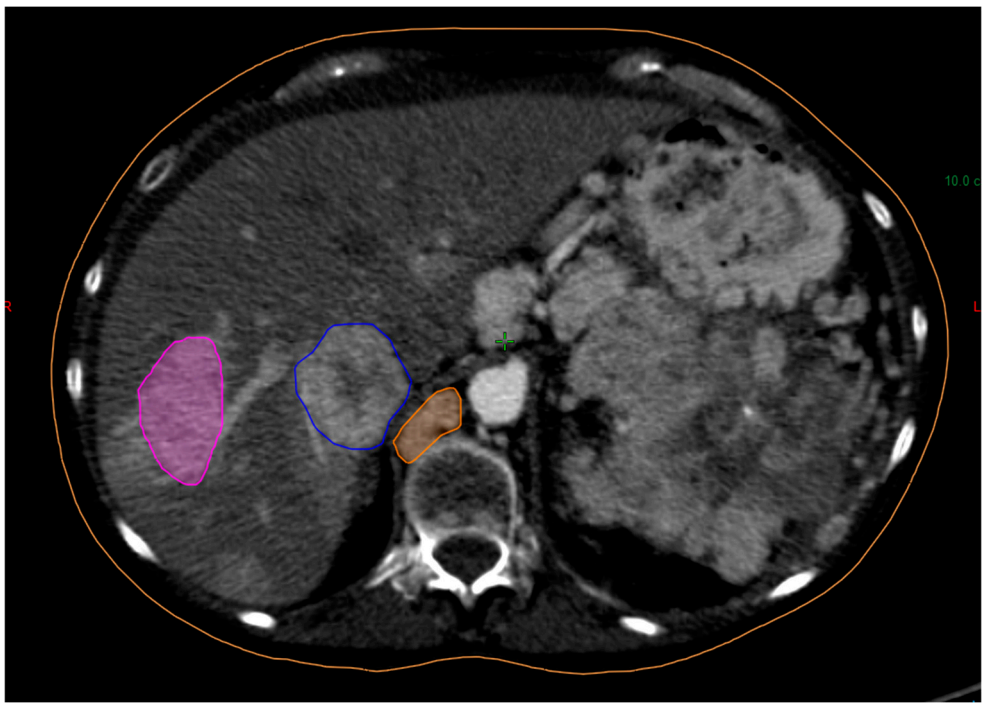

Figure 6. Transversal CECT image of a patient with metastasized NET. Tumor lesions, here two liver lesions and a paraaortic lymph node conglomerate, were manually delineated in subsequent 2D transversal images, creating a 3D VOI

Paper IV

Material was derived from the ILUMINET trial. Subjects from both Lund and Gothenburg were included. Eligibility in this sub study required that patients were untreated with PRRT prior to inclusion in the ILUMINET trial. The tumor burden was automatically delineated into VOIs using a software which is under development at our center, based on SPECT from cycle 1. The VOIs were manually compared to diagnostic images by an experienced clinical oncologist to confirm their correspondence to malignant lesions. If the SPECT or diagnostic images were ambiguous or of limited quality, the patient was excluded. When appropriate, VOIs were manually altered, deleted or added. Dose-rates were acquired from SPECT and absorbed doses calculated using half-lives derived from Paper II (103 and 81 hours for G1- and G2-tumors, respectively). For subsequent cycles, VOIs were generated by co-registering the approved VOIs from cycle 1 to those delineated for the new SPECT images. VOIs that did not harmonize with those of cycle 1 were rejected. For remaining cycles, a 2-dimensional rendering of the SPECT image with VOIs overlaid were inspected by an experienced medical physicist with support from an experienced oncologist and compared with those from cycle 1. In case of ambiguities, VOIs were inspected in the 3D SPECT image. Individual tumor absorbed doses were mass weighted before averaging, that is, the volume and deposited energy of the entire delineated volume was combined before conversion to mean absorbed dose across the tumor burden. Survival data were obtained from the ILUMINET database, last updated on 30 November 2019.

Statistical considerations

Paper I

For the survival analysis, Kaplan-Meier curves were used to illustrate survival times for both the entire population and across subgroups. Log-rank test was utilized to test survival differences between subgroups. In retrospect, however, we should have been clearer in the presentation of the tests made. In the abstract, the following sentence might be misleading:

"*The median PFS and OS were 29 months and 47 months, respectively, and were significantly associated with kidney dose, performance status, and Ki 67 levels but not with tumor origin*"

This implies that statistical significance pertains to differences in median survival times. However, as stated in the statistical methods section:

"*Kaplan–Meier curves were used to evaluate progression-free and overall survival, and log-rank tests were employed to assess differences between subgroups.* "

However, the log-rank test does not evaluate differences in median survival but rather tests the null hypothesis that survival distributions are identical across groups (109). This misinterpretation was further reinforced in Figures 1b–d and 2b–d, where p-values from log-rank tests are presented alongside dashed lines indicating median survival times. This visual pairing may be interpreted as if the p-values refer to differences between medians, which is incorrect. Additionally, a significant log-rank test indicates that at least one group differs significantly from another but does not specify which groups differ or whether all groups are separated. This nuance was not clearly conveyed in figure captions or text. To estimate confidence intervals for proportion the Wald method was used. All statistical analyses were done using R version 4.0.2

Paper II

In this paper, linear mixed models were used to evaluate changes in dosimetric quantities across treatment cycles, stratified by tumor grade. These models were chosen over simple regression to account for potential covariance among measurements from tumors within the same patient, and between patients having the same tumor grade (G1 or G2). The linear mixed models were specified with random intercepts and slopes for entities (in this case, tumors) nested within higher-level categories (in this case, patients). This allowed the model to account for intra-patient correlation and variability in dosimetric quantities across treatment cycles. Rather than fitting a single curve to all data points, the model estimated variance components at both the patient and tumor level, thereby adjusting for category-dependent biases.

To assess the differences between exploratory and reference methods (full dosimetry) for calculating cumulative absorbed dose, Bland–Altman plots were constructed. Limits of agreement were defined as ±2 standard deviations (SD) of the relative difference between the exploratory and reference method. To account for both inter- and intra-patient variability, the SD was estimated using one-way ANOVA. Statistical analyses were done using R, version 4.0.2.

Paper III

Inspired by the definitions of response in RECIST 1.1, tumors with a volume-reduction of 66 % were defined as responders. RECIST defines a partial response as a decrease of the sum of longest diameters of a set of predetermined tumors by 30 %. A diameter reduction of 30 % gives a 66% reduction of a corresponding sphere. With the purpose of increasing the number of observations, a different cut-off (4 cm^3) for tumor volume was chosen compared to Paper II. The uncertainties of the absorbed dose calculations (which increase with decreasing volume due to the partial volume effect) were estimated at different volume thresholds (110) and

were propagated into subsequent analyses. To account for intra-patient variability, linear mixed models were used to compare absorbed dose means between responders and non-responders stratified for tumor grade. If the means of a variable differed significantly between non-responders and responders, this variable was subjected to further analysis using non-linear mixed models.

This included logistic regression to assess the tumor control probability (TCP) as a function of cumulative absorbed dose, using the dichotomized responder and non-responder groups as the outcome variable. To assess the model's ability to accurately predict outcomes, a receiver operating characteristic (ROC) curve was created based on the TCP model. Area under the curve was calculated to assess the model's ability to distinguish between responders and non-responders and Youden's index was calculated to find the absorbed dose level that best separated responders and non-responders (111).

In addition, a non-linear regression using an asymptotic growth model to predict tumor shrinkage (%) as a continuous function of cumulative absorbed dose was used.

All statistical analyses were done using R version 4.2.2, with packages for mixed models and ROC (112, 113).

Paper IV

For statistical analysis, patients were dichotomized according to the median absorbed dose for cycle 1 and cumulative dose, respectively. Kaplan-Meier curves and log-rank test were used to estimate survival difference between subgroups. Cox regression was performed for estimations of hazard ratios (HR) between subgroups both in an univariable and a multivariable model. Log-log curves were visually inspected for all included variables to verify that hazards were proportional throughout the observed time span. For a visualization of the factors potentially confounding the relation between exposure and outcome a directed acyclic graph was created. To facilitate model robustness, the number of variables were limited to *circa* one per ten events. Despite some discrepancy between the number of PFS and OS events, the same set of variables were included in both analysis, after checking that the number of events per variable was within reasonable limits (114). Categorical values were denoted as such in SPSS and the exposure (AD for Cycle 1 and cumulatively, respectively) were chosen as reference. The enter method was used. The study population was also divided into absorbed-dose quartiles and analyzed for survival difference as outlined above. SPSS version (IBM) 20.0.0.0 was used for all calculations.

Use of Generative AI

Generative AI has been used throughout the thesis process to support writing and language refinement. Specifically, I have used Microsoft Copilot to assist with drafting and improving clarity. Suggestions provided by the AI have been critically reviewed and verified against primary sources and scientific literature before inclusion.

Results

Paper I

In total, 103 patients were included in the study. Six patients had received PRRT previously and were therefore excluded from the statistical analyses. One patient withdrew consent. Hence, 96 patients were included in the final analysis.

Seven patients died and 12 had progressive disease before reaching an accumulated 27 Gy BED and an additional 13 stopped treatment because of toxicity. Of the 64 patients completing Step 1, 9 patients entered Step 2 (treatment to an accumulated BED of 40 Gy). The distribution of number of treatments is shown in Figure 7.

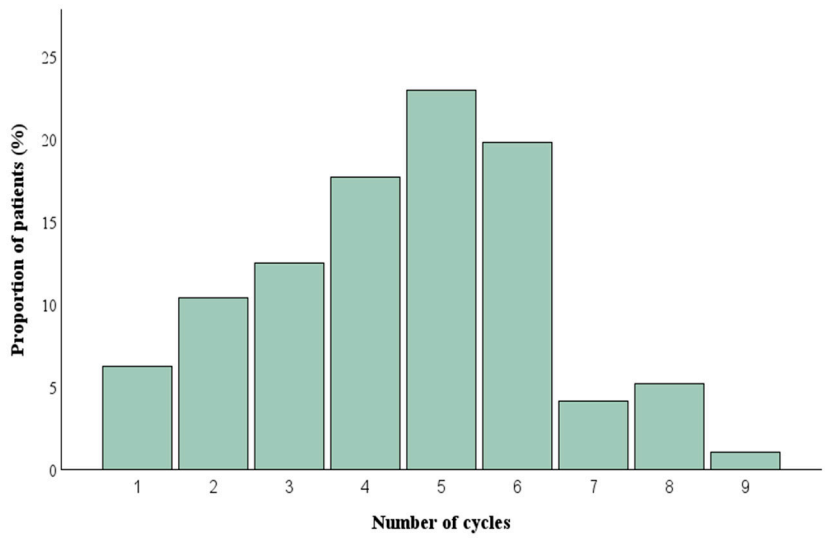

Figure 7. Histogram of the frequence distribution of treatment cycles. Note that a majority (53%) were given more cycles than the standard protocol (4). Created in SPSS 20.0.0.0 (IBM).

The best overall response was 2% complete response, 32% partial response, 61% stable disease, and 4% progressive disease.

The median time until disease progression was 29 months, while the median overall survival reached 47 months. Patients with better performance status, lower Ki-67

proliferation index, and higher kidney BED tended to have more favorable outcomes. Primary tumor site did not significantly influence survival.

Adverse effects were generally mild. The most frequently reported side effects included fatigue, nausea, and hematologic changes such as anaemia and reduced platelet counts. Severe toxicity (grade 3–4) was uncommon, affecting fewer than 10% of patients, and no serious kidney-related toxicity was observed. Two individuals developed acute myeloid leukemia during long-term follow-up, both had received only somatostatin analogs prior to PRRT.

Among those eligible for extended treatment into Step 2, no severe adverse events were recorded, and kidney function remained largely preserved.

Paper II

Tumors from a total of 41 patients were included. Dosimetry was performed for 182 tumors, resulting in 880 individual assessments. Five dosimetric parameters were analyzed, all with different inclusion criteria rendering some variation in the number of tumors included and temporal observations made.

Tumor absorbed dose (AD) was estimated for 109 tumors in 39 patients through 404 individual assessments. The AD distributions across all tumors, stratified for tumor grade, are shown in Table 6.

Table 6

Tumor absorbed dose (AD) per cycle and cumulative AD over all delivered cycles.

Category	Per cycle, per tumor, all patients	Per cycle, G1 (median across tumors in each patient)	Cumulative, G1	Per cycle, G2 (median across tumors in each patient)	Cumulative, G2
Median across patients (Gy)	19	21	137	13	80
Range (Gy)	2–77	3.5–66	33–403	4.7–32	11–211

Through linear mixed-effect models, estimations of how the dosimetric parameters evolved over treatment cycles were made. They are showcased in Table 7.

Table 7 The development of dosimetric parameters from one cycle to the next for G1 and G2 tumors. P-values indicate the probability that G1 and G2 are the same.

	Mean percentual change from one cycle to the next with 95% CI for G1 tumors		Mean percentual change from one cycle to the next with CI 95% for G2 tumors		p
Activity concentration (MBq/mL)	-6.1	-11 to 0.89	-14	-20 to 8.4	0.04
Absorbed-dose rate (mGy/h)	-6.2	-11 to 0.89	-14	-20 to 8.3	0.04
Effective half-time (h)	-0.69	-2.1 to 0.77	-1.2	-3.4 to 1.1	0.7
Volume (cm^3)	-1.1	-5.0 to 3.0	-6.4	-11 to -1.4	0.1
Absorbed Dose (Gy)	-5.7	-11 to -0.12	-14	-20 to -7.9	0.04

As observed, the AD diminishes throughout cycles, significantly more so for G1 than G2 tumors. This is due to a decrease in absorbed dose rate which is ultimately dependent on the activity concentration since the half-life is virtually stable. Notably, the effective half-lives differed significantly between G1 (103 h; 95% CI, 96–109 h) and (81 h; 95% CI, 73–90 h) for G2.

Three potential methods for simplification of dosimetry schemes were evaluated for accuracy with the full dosimetry schemes as reference, Table 8.

Table 8 Results of three methods for dosimetry simplification compared to full dosimetry.

Method for simplification	Means (%)	Limits of Agreement
Using constant AD/cycle, from first cycle	15	55
Using constant effective half-life, from first cycle	0.43	13
Using constant effective half-life, global means*	0.01	31

* 103 h for G1 and 81 h for G2 tumors

Paper III

Sixty-nine tumors from 32 patients were included in the final analysis. Of these, 41 were from patients whose latest biopsy showed G1 and 28 from patients whose latest biopsy showed G2. Median follow up time for the patients was 2.7 years with a range of 0.8 to 8.3. Volumetric and dosimetric data are summarized in Table 9.

Table 9. Median and range for volumetric and dosimetric parameters the number of responders. Cumulative absorbed dose is the total dose delivered up to the point of best tumor response.

Parameter	All Tumors	G1 Tumors (n=41)	G2 Tumors (n=28)
Baseline volume (cm^3)	17.1 (4.0–630)	14.6 (4.4-585	21.9 (4.0-630)
Tumor volume reduction (%)	69.9 (6-100)	63 (13-100)	75 (6-100)
Cumulative tumor AD (Gy)	142 (22–368)	179 (35–368)	109 (22–226)
Responders/non-responders (n)	40/29	20/21	20/8

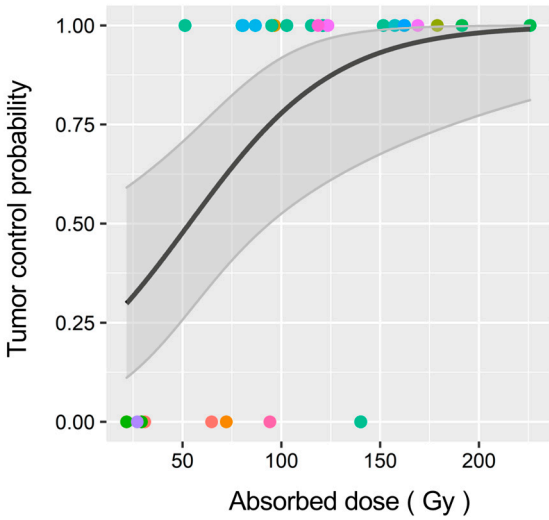

Figure 8. Logistic regression analysis of the tumor control probability at different cumulative absorbed doses. Gray shading indicates 95 % confidence intervals The colored dots represent responding or non-responding tumors. This figure was originally published in Paper III.

For the total tumor population, regardless of grade, responding tumors had a mean AD of 165.8 Gy and non-responding tumors 143.7 Gy. For G1 tumors, responding tumors and non-responding tumors had mean AD of 203 and 163 Gy respectively while responding and non-responding G2 tumors had mean AD of 128 and 68 Gy respectively. Linear mixed effect models showed that the mean AD between responding tumors and non-responding tumors (tumor shrinkage differed significantly for G2 tumors ($p = 0.01$) but not for G1 tumors ($p=0.08$).

For G2 tumors, logistic regression was performed to analyze TCP at different absorbed-dose-levels. This absorbed-dose-response relationship was supported by ROC analysis, which yielded an area under the curve of 0.89, indicating strong predictive performance. To identify the most discriminative threshold for TCP, Youden's J statistic was applied. The optimal threshold was found to be 65% (76 Gy), corresponding to a sensitivity of 0.95 and a specificity of 0.75. This threshold represents the point at which the balance between true positive and false positive classifications is maximized.

Paper IV

For analyses with the mean AD from the entire tumor burden of Cycle 1 as the explanatory variable, 81 patients were included while 80 were included for analyses with the cumulative mean AD from the entire tumor burden as the explanatory variable.

Kaplan-Meier curves and log-rank tests revealed that patients with tumor mean-AD over the cohort median had significantly better PFS and OS, than patients with tumor mean-AD below the median, both with respect to the AD in cycle 1 and the cumulative AD. This was confirmed in univariable Cox regression, Table 10.

Table 10. Hazard ratios and 95 % confidence interval between tumors with high and low mean-AD. All analyses had a p value < 0,05.

	PFS	OS
AD Cycle 1, HR (95 % CI)	0.51 (0.30-0.86)	0.53 (0.29-0.99)
Cumulative AD, HR (95 % CI)	0.42 (0.24-0.73)	0.50 (0.27-0.93)

Multivariable Cox regression confirmed that tumor mean-AD for cycle 1 and the cumulative AD were independent predictors of survival, even after adjusting for performance status, prior treatments, age, and tumor grade (Table 11).

Table 11. The HR and 95% confidence intervals for parameters in a multivariable Cox regression model. Significant results are denoted with a star.

	AD, Cycle 1		AD, Cumulative	
	PFS, HR (95% CI)	OS, HR (95% CI)	PFS, HR (95% CI)	OS, HR (95% CI)
Tumor mean-AD (high vs low)	0.34 (0.19-0.63) *	0.41 (0.21-0.81)*	0.37 (0.21-0.66)*	0.48 (0.25-0.93)*
Tumor grade (1 vs 2)	0.97 (0.56-1.70)	1.08 (0.56-2.08)	1.04 (0.61-1.80)	1.18 (0.62-2.27)
ECOG (0 vs ≥ 1)	0.48 (0.27-0.85) *	0.47 (0.25-0.89) *	0.53 (0.30-0.94)*	0.49 (0.26-0.94)*
Previous treatment (no vs yes)	0.38 (0.21-0.69)*	0.32 (0.16-0.67)*	0.40 (0.22-0.73)*	0.33 (0.16-0.69)*
Age	0.95 (0.92-0.98)*	0.97 (0.94-1.00)	0.96 (0.93-0.98)*	0.98 (0.95-1.01)

To further examine the effect of mean-AD on the survival distribution, the population was divided into quartiles based on their AD and investigated for survival differences with Kaplan-Meier curves and log rank test. For cumulative AD, log rank test showed that the survival distribution of the highest quartile

(cumulative AD > 118 Gy) significantly differed to the other quartiles; both when tested individually (*e.g.* 1st vs 4th) and when tested against the other quartiles as a single group. This held true for both PFS and OS.

Table 12. Comparison of PFS and OS between AD quartiles. p-values are derived from log-rank tests and hazard ratios with 95 % confidence intervals derived from cox regressions.

	PFS, p	OS, p	PFS, HR (95 % CI)	OS, HR (95 % CI)
Q4 (> 118 Gy) **vs Q1** (≤ 46 Gy)	<0.001	0.003	0.16 (0.06-0.42)	0.23 (0.08-0.66)
Q4 (> 118 Gy) **vs Q2** (47-74 Gy)	0.003	0.024	0.29 (0.12-0.68)	0.33 (0.12-0.91)
Q4 (> 118 Gy) **vs Q3** (75-118 Gy)	0.007	0.039	0.33 (0.14-0.77)	0.33 (0.12-0.99)
Q4 (> 118 Gy) **vs Q1-Q3** (≤118 Gy)	<0.001	0.006	0.25 (0.12-0.54)	0.29(0.12-0.75)

To evaluate the independence of the 118 Gy threshold, the cut-off was included in the multivariable model, yielding HRs (95 % CI) of 0.27 (0.13-0.59) and 0.28 (0.11-0.73) for PFS and OS, respectively.

Higher tumor mean-ADs did not correlate with increased toxicity. The frequency of grade ≥3 adverse events was similar across AD quartiles.

Discussion

"The best workout is the one completed"

Per Warfvinge, Swedish lawyer

Paper I

Our data strongly indicate that dosimetry-guided individualization of the number of treatment cycles of ^{177}Lu-DOTA-TATE is safe. Despite the majority of patients receiving more than the clinically standard four cycles, no grade 3–4 toxicity occurred. This aligns well with long-term retrospective cohorts, which do not show a notable proportion of serious renal side effects from Lu-PRRT (74-76). Fewer patients than intended were included in step 2 (treatment to renal BED of 40 Gy), somewhat limiting the safety information in these higher BED range.

Ten percent of patients experienced grade 3–4 hematological side effects, which in most cases were transient. However, two patients developed therapy-related myeloid neoplasms (tMN). This is comparable to other PRRT studies, where approximately 2% of patients developed tMN (115), after a mean latency time of 41-57 months (75, 76). Thus, there is no obvious indication that increasing the number of treatment cycles escalates the risk of tMN. In a dosimetry-guided Canadian study that altered the administered activity per treatment cycle, a higher proportion of hematological side effects was observed, including a 5% rate of persistent neutropenia (93). Indeed, a dose–response relationship appears to exist between bone marrow AD and hematological toxicity (116, 117). However, in a large retrospective Dutch study (118) with 11 cases of tMN, no correlation between estimated bone marrow AD and risk for tMN was seen.

Safety aside, it is inevitable to compare the efficacy results to the NETTER-1 trial (29) which established the now clinically approved standard protocol of 4 × 7.4 GBq cycles. While a definitive comparison between individualized and non-individualized PRRT is not possible outside the framework of a randomized multi-arm study, the efficacy numbers are worth reflecting upon. Of special note, the proportions of patients with Grade 1 and Grade 2 differ, with a higher proportion of the ILUMINET patients having Grade 2 disease. Median PFS and OS in NETTER-

1 were similar, while the overall response rate (ORR) was higher in ILUMINET (34% compared to 18% in NETTER-1), see Table 13.

Table 13. Median survival times, objective response rate and distribution of grade 1 and grade 2 patients in ILUMINET and the exploratory (PRRT) arm of NETTER-1

	ILUMINET	NETTER-1
PFS, months	29	28[119]
OS, months	47	48
ORR, %	34	18
G1/G2, %[120]	38/62	66/35

It should be noted, however, that ORR does not necessarily translate to improved survival (121, 122), and the value of this parameter should be interpreted cautiously.

In conclusion, this study further substantiates the notion that kidney toxicity is not a major limiting factor in PRRT with ^{177}Lu. However, no definitive clinical benefit of individualization by increasing the number of cycles was observed, highlighting the need for even more refined dosimetry-guided treatment schemes.

Paper II

In this study, we demonstrate several key concepts, important for future treatment dosimetry protocol design.

Firstly, there is substantial variability in tumor AD between tumors and patients, consistent with the known biological heterogeneity of the disease(123). This strengthens the case for individualized treatment strategies, given that the same administered activity can result in markedly different amounts of radiopharmaceutical delivered to the tumors. Secondly, the tumor AD to NETs (particularly to G2 tumors) decreases over successive treatment cycles with ^{177}Lu-DOTA-TATE. The decline is primarily due to reduced uptake of the radiopharmaceutical in the tumors. This harmonizes well with observations that radiation-induced fibrosis arises in pNETs (most of whom are G2 in our material) after PRRT (124), a plausible while not proven explanation. Grade 1 tumors show a less pronounced decrease, potentially due to lower rates of proliferation and cell death. Given our and other groups' (99, 125, 126) observation that tumor absorbed dose diminishes through sequential PRRT cycles, the key question is how the treatment strategy should be adapted. One could argue for administering higher activities during the initial cycles, when the tumor appears more receptive to radiopharmaceutical uptake, or alternatively for administering higher activities in

the later cycles to ensure an optimal cumulative tumor dose. Of note, the tumor-to-kidney ratio decreases across cycles, both in our study and a similar from the University of Michigan (126). underscoring the need for caution regarding accumulated kidney absorbed dose if the latter approach is considered. Thirdly, the effective half-time of the radiopharmaceutical remains relatively stable across cycles. This observation suggests that simplified dosimetry protocols could be feasible. When comparing full dosimetry with a simplified method using the half-life from the first cycle, the limits of agreement, reflecting the degree of individual variation, were 13 %. This indicates that simplified schemes, omitting repeated measurements for half-life estimation, saving time for both patients and staff.

Our study has several limitations. First, although the data were collected prospectively, the curation and analysis were performed retrospectively, which inevitably introduces a risk of selection bias. Furthermore, the dosimetry protocol was optimized for kidney dose estimation and relied on planar imaging to determine effective half-times. When a tumor overlapped with another lesion, a kidney, or the spleen in the anteroposterior projection, accurate determination of that lesion's half-life was impossible. Consequently, these tumors were excluded from analyses that depended on half-time estimation, including absorbed dose, possibly introducing a bias.

On balance however, our study provides robust data indicating that tumor AD declines markedly across successive PRRT cycles, a finding with major implications for the design of future dosimetry-guided studies. We also show that variability in tumor AD between patients and lesions supports a move toward individualized therapy, and that accurate AD estimation can be achieved with simplified dosimetry protocols.

Paper III

This study provides important insights into the relationship between AD and tumor response in NET treated with ^{177}Lu-DOTA-TATE. Responding G2 tumors generally received higher cumulative ADs compared to nonresponders, whereas this trend was less pronounced and not statistically significant for G1 tumors. These observations align with previous reports suggesting a stronger dose–response relationship in pancreatic NET and a weaker association in small-intestinal NET (97, 127), which are typically slower-growing.

A key result was the identification of a potential AD threshold for achieving high TCP. Modeling suggested that an accumulated AD of approximately 135 Gy corresponds to a TCP of 90% for G2 tumors, a value that potentially could be used as a benchmark in future tumor dosimetry-guided treatment schemes. However, an important question is whether optimal patient benefit comes from tumor shrinkage

per se given that tumor response is not an immediate predictor of improved survival. On the other hand, patients with NET have a worse health-related quality of life (HRQoL) than the general population(128) and it has been suggested that overall response rate after PRRT correlates with improves HRQoL (129) even though total tumor burden does not seem to correlate with HRQoL. (130).

Several limitations must be acknowledged. The retrospective design and relatively small sample size restrict generalizability, and the exclusion of tumors with a volume below 4cm3 leaves unanswered questions regarding the dose-response relationship in small tumors. Additionally, volumetric assessments were performed manually by a single observer, introducing potential bias. The decision to exclude tumors that progressed during treatment involved a balance of considerations. One argument for their exclusion was that PRRT often requires time to exert its therapeutic effect(98), and that neuroendocrine tumors can be intrinsically radioresistant(131). Including such tumors, unlikely to respond under any circumstances, could have introduced noise into the analysis. Despite these constraints, the results are consistent with prior studies and support the clinical relevance of AD as a key determinant of response.

In conclusion, our study reinforces the concept that individualized dosimetry could optimize peptide receptor radionuclide therapy. Targeting an AD of at least 135 Gy for G2 tumors may improve outcomes, though further prospective studies are needed to validate these findings and refine treatment protocols.

Paper IV

This study demonstrates that the mean AD to the entire tumor burden is a strong and independent predictor of survival in patients with grade 1-2 NET treated with ^{177}Lu-DOTA-TATE. Analyses were performed with regards to both cumulative AD and the AD of cycle 1. Previous research has suggested a link between tumor AD and clinical outcomes, but most studies were limited by small cohorts, short follow-up, or reliance on selected lesions rather than whole-tumor-burden dosimetry (99-101). By addressing these limitations, our findings provide more robust evidence that higher tumor mean-AD correlates with improved PFS and OS.

Survival benefits were observed both when patients were grouped by median AD and, for the analyses of cumulative AD, when stratified into quartiles. Notably, patients in the highest quartile (>118 Gy cumulative AD) had markedly better outcomes without an increase in severe toxicity. This supports the concept of a clinically relevant threshold for tumor AD, which roughly aligns with values reported in some earlier studies, see Table 14. It shall however be noted that some studies have found distinctively lower cut-off points being indicative of survival benefits.

Table 14. Overview of studies investigating the relationship between tumor AD and survival.

Author (Year)	Treatment	Cut-off (Gy)	Clinical Outcome	AD from
Hebert et al. (2024)	^{177}Lu-PRRT	91.36 (mean), 52.52 (lowest)	Improved PFS; OS trend	Cumulative
Mileva et al. (2024)	^{177}Lu-PRRT	35 (lowest)	Improved PFS	Cycle 1
Maccauro et al. (2024)	^{177}Lu-PRRT	10.6 (mass-weighted mean)	Improved PFS	Cycle 1
Warfvinge et al. (Paper IV)	^{177}Lu-PRRT	118 (mass-weighted mean)	Improved PFS and OS; no ↑ toxicity	Cumulative
Ebbers et al. (2022)	^{90}Y-SIRT	101 (mean)	Disease stabilization	Cumulative

These studies also highlight the need for standardization in dosimetric practice. Current approaches differ in whether they use minimum AD, arithmetic mean AD, or mass-weighted mean AD, and in how tumors are selected for analysis. Establishing consensus on these aspects, as well as imaging protocols for tumor identification, will be essential for translating dose-response evidence into clinical guidelines.

Our study has several limitations. The analysis was retrospective, although based on prospectively collected trial data, and fixed effective half-lives were used for dose calculations. This infers uncertainty to the results that is hard to value quantitively. Importantly though, the half-lives used (103 h for G1 and 81 h for G2, respectively) are close to the corresponding values reported in an American analysis (111 h and 93 h) (126). The underlying causality must also be addressed: while our multivariable analyses adjusted for tumor grade and prior treatment lines (as best available proxies for tumor differentiation and aggressiveness), it is yet to be established whether the observed association between higher tumor AD and improved survival reflects a true causal relationship. Tumor grade was determined from biopsy samples, which in some cases were several years old and may therefore not accurately represent the biological behavior of the disease at the time for treatment start. Consequently, it is plausible that patients with higher-differentiated tumors, characterized by higher somatostatin receptor expression, both accumulate more radiolabelled peptide and have a more favorable prognosis. In this scenario, the survival benefit associated with higher tumor AD may not be solely attributable to the AD itself, but rather to a shared biological trait that influences both radiotracer uptake and disease progression.

Nevertheless, our study contributes important pieces of information to the question of how AD contributed to patient survival, not least by our wholetumor burden dosimetric approach and state-of-the art survival analyses.

Future perspectives

The overarching theme of this thesis has been to contribute to the understanding of how to individualize PRRT through dosimetry. This has been achieved by exploring data from our phase II study on kidney dosimetry and subsequently exploring our considerable data set to conduct post-hoc analyses focusing on tumor absorbed dose. Our findings regarding kidney dose are consistent with previous studies and conclude that renal BED up to and exceeding 29 Gy are safe.

While our results are not methodologically robust enough to independently establish that tumor absorbed dose is a key determinant of survival, they harmonize well with other studies. Assuming that the relationship is causal, how should dosimetry be used to guide treatment in a hypothetical multi-arm randomized study designed to compare dosimetry-guided and standard treatment schemes?

If the administered activity is to be guided by tumor absorbed dose, several critical aspects must be addressed. The first decision to make is which absorbed-dose metric and measurand should be used. Presently, this is unclear.

Second, the choice of a reference value for dose adjustment must be established. Thirdly, the practical means to moderate the absorbed doses would need to be considered. One approach could be to administer a uniform activity in the first cycle for all patients, followed by dosimetry and individualized adjustment of the number of cycles or the administered activity in subsequent cycles. A Swedish randomized multicenter is currently exploring the survival differences between standard and dosimetry guided number of treatment cycles (132). This method has the advantage of simplicity and circumvents the lack of established techniques for pre-treatment AD estimation. However, it also has theoretical drawbacks, notably the tendency for tumor AD to decrease across treatment cycles(125-127, 133).

While ^{68}Ga-DOTA-TATE PET seems to predict renal absorbed dose to the kidneys with reasonable accuracy(134), estimating tumor AD before therapy remains a challenge. PET imaging with ^{68}Ga-DOTA-SSTR has been explored to assess whether pre-treatment uptake correlates with absorbed dose from ^{177}Lu-DOTATATE. While moderate correlations have been observed at the population level, the predictive accuracy for individual tumors lacks precision (135-137). This limitation is partly due to the significant difference in physical half-lives between the isotopes, 68 minutes for ^{68}Ga and 6.6 days for ^{177}Lu, resulting in divergent pharmacokinetics. An avenue for future research could be to evaluate the ability of

novel ^{18}F-labeled somatostatin receptor tracers (which has somewhat a longer half-life than ^{68}Ga) to individually predict the tumor AD in the first treatment. In contrast to other options (such as ^{86}Y-SSTR-PET with an even longer half-life) ^{18}F-SSTR-PET has also proven to be a robust diagnostic tool (138) potentially increasing the incentive to introduce the method broadly. Another concept worth exploring is the administration of a trace dose of ^{177}Lu prior to therapy, analogous to the use of diagnostic ^{131}I in the treatment planning for hyperthyroidism. Such an approach could enable individualized dosimetry before therapeutic administration, potentially improving treatment precision and outcomes.

Populärvetenskaplig sammanfattning

Neuroendokrina tumörer (NET) är cancersjukdom som uppstår från en speciell typ av celler som kallas för neuroendokrina celler. Neuroendokrina celler har i sitt friska tillstånd som uppgift att producera hormoner som kroppen behöver för att reglera olika funktioner. Exempel på neuroendokrina celler är de celler i bukspottkörteln som insulin (för att sänka kroppens blodsockernivåer) och de celler i binjuren som producerar adrenalin.

Precis som alla celler i kroppen kan även neuroendokrina celler bli cancer. Detta sker genom att de (till följd av mutationer i sitt DNA) skaffar sig förmågan att dela sig ohämmat, invadera omgivande vävnader och sprida sig i kroppen. Den sjukdom som du uppstår kallas NET. Om man finner NET i tid kan man bota sjukdomen genom att operera bort den. Om den däremot hunnit sprida sig i kroppen kan man i de allra flesta fall inte bli av med sjukdomen, utan den behandling som då ges syftar i stället till att se till att patienten som drabbats lever så länge och så bra som möjligt med sjukdomen.

En metod att behandla obotlig NET är genom *radionuklidterapi*. Det fungerar genom att man injiceras ett ämne där en *somatostatinanalog* har kopplats till ett radioaktivt ämne, ^{177}Lutetium. Somatostatinanaloger är ett ämne med förmågan att fastna på neuroendokrina celler inklusive de flesta NET. När somatostatinanalogen är kopplad till det radioaktiva ^{177}Lutetium kommer därför detta att hamna där NET finns. ^{177}Lutetium skickar ut två typer av radioaktiv strålning. Den första kallas β-strålning. Den färdas någon tiondels millimeter från ^{177}Lutetium innan den bromsas upp och absorberas. De strukturer den träffar på sin färd skadas och det är så radionuklidterapi ger sin effekt på cancer. Den andra typen kallas γ-strålning. γ-strålning färdas flera meter från ^{177}Lutetium, men ställer inte till tillnärmelsevis lika mycket skada i kroppen. Den kan dock detekteras med en så kallad gammakamera vilket gör att man kan mäta var och hur mycket ^{177}Lutetium som hamnat på olika ställen i kroppen. Detta kallas dosimetri.

Radionuklidterapi med ^{177}Lutetium är ett godkänt läkemedel och används i vården av patienter med NET. I ”vardagen” får alla patienter samma dos och antal behandlingar. Många forskare runt om i världen misstänker dock att medicinen hade kunnat få än bättre effekt genom att mäta hur mycket ^{177}Lutetium som hamnar i tumörerna och njurarna (det organ från vilket man är orolig för biverkningar) för varje patient och styra antal behandlingar eller vilken dos man ger därifrån

För att kunna veta *hur* man skall styra behandlingen måste man dock känna till hur tumörer och njurar reagerar på olika stråldoser. Syftet med den här avhandlingen har varit att utforska sambandet mellan stråldos och effekter i tumörer och njurar.

Arbete I

Arbete I beskriver resultaten av den forskningsstudie (ILUMINET-studien) som ligger till grund för alla arbeten i avhandlingen. I studien behandlades 103 patienter med radionuklidterapi. Efter varje behandling mättes stråldosen till njurarna med hjälp av dosimetri. Så länge den totala stråldosen låg under ett förutbestämt värde och man inte mådde dåligt fick man fortsätta behandlingen. Slutresultatet blev att patienterna i studien fick fler behandlingar (i genomsnitt fem) än de fyra som man får i vanliga fall. Därtill fick inte patienterna några svåra njurbiverkningar. Vi tolkar resultaten som att det är säkert att ge fler behandlingar än de rekommenderade fyra så länge man noggrant mäter stråldosen i njurarna.

Arbete II

I det här arbetet använde de mätningar som gjort inom ramen för ILUMINET för att mäta stråldosen till de tumörer som patienterna hade. Vi beräknade stråldosen för ett stort antal för att fastställa hur den varierade inom tumörer hos samma patient och mellan behandlingstillfällena. Vi såg att mer snabbväxande tumörer får en betydligt högre stråldos vid de första behandlingstillfällena. Detta kan vara en viktig observation när man skall designa framtida behandlingsprotokoll. Om det är så att lejonparten av den totala stråldosen kommer från de första behandlingsomgångarna kanske man behöver öka den givna dosen i de sista.

Arbete III

I de här arbetet undersökte vi om stråldosen i enskilda tumörer påverkade hur mycket de krympte. Vi såg att snabbväxande tumörer som krympte mycket hade fått en högre genomsnittlig stråldos än de som krympte mindre. Vi uppskattade också vilken stråldos som behövs för att en viss andel av tumörerna skall krympa. Vi tolkar resultaten som ett stöd för att hypotesen att stråldos spelar roll för tumöreffekt stämmer. Dessutom är det av stor nytta att vi kommit ett förslag på vilka stråldoser som ger vilken krympningseffekt.

Arbete IV

I det här arbetet uppskattade vi stråldosen till den totala mängden tumörvävnad i varje patient. Vi undersökte därefter om de patienter som fått en högre stråldos levde längre tid än de som fått en lägre stråldos. Vi såg att de patienter som fått en högre stråldos generellt levde längre än de som fått en låg stråldos, utan att de för den sakens skulle få fler biverkningar. Detta tolkar vi som ett kvitto på att stråldosen spelar roll för det allra viktigaste för patienterna: Hur länge och bra de lever.

My contributions

Paper I	I contributed to data collection, interpretation of data, writing and revising.
Paper II	I contributed to data collection, interpretation of data and writing and revising
Paper III	I contributed to conceptualization, methodology, data collection, interpretation of data, writing, revising and submitting as corresponding author
Paper IV	I contributed to conceptualization, methodology, data collection, statistical analysis, and writing.

Acknowledgements

I am deeply thankful for having been granted the opportunity to do such a enriching and fun project as this. Specifically, I want to express my gratitude to:

My main supervisor **Katarina Sjögreen Gleisner**. Thank you for taking me under your wings and providing me with the opportunity to make this thesis. You are patient yet determined, humble yet immensely knowledgeable, thorough yet effective. You have contagious curiosity, steadfast scientific integrity and impressive grit. Thank you for this time, and (if you find it worthwhile) I would really like to continue to work together.

My brilliant, visionary and enthusiastic co-supervisor **Anna Sundlöv**. You were instrumental in making this opportunity possible, and you have guided me with kindness, honesty, and genuine engagement.

My co-supervisors **Michael Ljungberg** and **Adalsteinn Gunnlaugsson** for help and guidance.

My co-worker **Johan Gustafsson** for being an all-around well of wisdom and a foundational pillar for this thesis.

My other **co-authors,** whose inspiration and dedication made this work possible.

My closest clinical colleagues, **Pernilla Asp** and **Karin Lideke**. Thank you for being such wonderful people and for never complaining or making me feel guilty for being away so often and for so long.

All my other **clinical colleagues**, from whom I have learned invaluable lessons about life and work, so often intertwined in oncology.

My **family and friends**.

Hanna Maria och **Hedvig** som gör livet roligt, meningsfullt och vackert. Jag älskar er.

References

1. MacDonald PE, Joseph JW, Rorsman P. Glucose-sensing mechanisms in pancreatic beta-cells. Philos Trans R Soc Lond B Biol Sci. 2005;360(1464):2211-25.
2. Quesada I, Tuduri E, Ripoll C, Nadal A. Physiology of the pancreatic alpha-cell and glucagon secretion: role in glucose homeostasis and diabetes. J Endocrinol. 2008;199(1):5-19.
3. Bauer W, Briner U, Doepfner W, Haller R, Huguenin R, Marbach P, et al. SMS 201–995: A very potent and selective octapeptide analogue of somatostatin with prolonged action. Life Sciences. 1982;31(11):1133-40.
4. Alcaino C, Guccio N, Miedzybrodzka EL, Quale JR, Lu T, Davison A, et al. Mechanisms of Activation and Serotonin Release From Human Enterochromaffin Cells. Cell Mol Gastroenterol Hepatol. 2025:101610.
5. Bellono NW, Bayrer JR, Leitch DB, Castro J, Zhang C, O'Donnell TA, et al. Enterochromaffin Cells Are Gut Chemosensors that Couple to Sensory Neural Pathways. Cell. 2017;170(1):185-98 e16.
6. Rindi G, Mete O, Uccella S, Basturk O, La Rosa S, Brosens LAA, et al. Overview of the 2022 WHO Classification of Neuroendocrine Neoplasms. Endocr Pathol. 2022;33(1):115-54.
7. Basuroy R, Bouvier C, Ramage JK, Sissons M, Srirajaskanthan R. Delays and routes to diagnosis of neuroendocrine tumours. BMC Cancer. 2018;18(1):1122.
8. Stensbøl AB, Krogh J, Holmager P, Klose M, Oturai P, Kjaer A, et al. Incidence, Clinical Presentation and Trends in Indication for Diagnostic Work-Up of Small Intestinal and Pancreatic Neuroendocrine Tumors. Diagnostics. 2021;11(11):2030.
9. Halperin DM, Shen C, Dasari A, Xu Y, Chu Y, Zhou S, et al. Frequency of carcinoid syndrome at neuroendocrine tumour diagnosis: a population-based study. Lancet Oncology. 2017;18:525-34.
10. Falconi M, Eriksson B, Kaltsas G, Bartsch DK, Capdevila J, Caplin M, et al. ENETS Consensus Guidelines Update for the Management of Patients with Functional Pancreatic Neuroendocrine Tumors and Non-Functional Pancreatic Neuroendocrine Tumors. Neuroendocrinology. 2016;103(2):153-71.
11. Fang JM, Li J, Shi J. An update on the diagnosis of gastroenteropancreatic neuroendocrine neoplasms. World J Gastroenterol. 2022;28(10):1009-23.
12. Bellizzi AM. Immunohistochemistry in the diagnosis and classification of neuroendocrine neoplasms: what can brown do for you? Human Pathology. 2020;96:8-33.

13. Rindi G, Mete O, Uccella S, Basturk O, La Rosa S, Brosens LAA, et al. Overview of the 2022 WHO Classification of Neuroendocrine Neoplasms. Endocrine Pathology. 2022;33(1):115-54.
14. Dasari A, Shen C, Halperin D, Zhao B, Zhou S, Xu Y, et al. Trends in the incidence, prevalence, and survival outcomes in patients with neuroendocrine tumors in the United States. JAMA oncology. 2017;3(10):1335-42.
15. Dasari A, Wallace K, Halperin DM, Maxwell J, Kunz P, Singh S, et al. Epidemiology of Neuroendocrine Neoplasms in the US. JAMA Netw Open. 2025;8(6):e2515798.
16. Thiis-Evensen E, Boyar Cetinkaya R. Incidence and prevalence of neuroendocrine neoplasms in Norway 1993–2021. Journal of Neuroendocrinology. 2023;35(4):e13264.
17. Ohlsson H, Nilsson M, Sundlov A, Malmstrom M, Almquist M. Quality of life as a predictor for survival in patients with small intestinal neuroendocrine tumours. J Neuroendocrinol. 2025:e70081.
18. Klomp MJ, Dalm SU, de Jong M, Feelders RA, Hofland J, Hofland LJ. Epigenetic regulation of somatostatin and somatostatin receptors in neuroendocrine tumors and other types of cancer. Reviews in Endocrine and Metabolic Disorders. 2021;22(3):495-510.
19. Günther T, Tulipano G, Dournaud P, Bousquet C, Csaba Z, Kreienkamp HJ, et al. International Union of Basic and Clinical Pharmacology. CV. Somatostatin Receptors: Structure, Function, Ligands, and New Nomenclature. Pharmacol Rev. 2018;70(4):763-835.
20. Eychenne R, Bouvry C, Bourgeois M, Loyer P, Benoist E, Lepareur N. Overview of Radiolabeled Somatostatin Analogs for Cancer Imaging and Therapy. Molecules [Internet]. 2020; 25(17).
21. Deppen SA, Liu E, Blume JD, Clanton J, Shi C, Jones-Jackson LB, et al. Safety and Efficacy of 68Ga-DOTATATE PET/CT for Diagnosis, Staging, and Treatment Management of Neuroendocrine Tumors. J Nucl Med. 2016;57(5):708-14.
22. Wolin EM. The expanding role of somatostatin analogs in the management of neuroendocrine tumors. Gastrointest Cancer Res. 2012;5(5):161-8.
23. Rinke A, Wittenberg M, Schade-Brittinger C, Aminossadati B, Ronicke E, Gress TM, et al. Placebo-Controlled, Double-Blind, Prospective, Randomized Study on the Effect of Octreotide LAR in the Control of Tumor Growth in Patients with Metastatic Neuroendocrine Midgut Tumors (PROMID): Results of Long-Term Survival. Neuroendocrinology. 2017;104(1):26-32.
24. Caplin ME, Pavel M, Ćwikła JB, Phan AT, Raderer M, Sedláčková E, et al. Lanreotide in metastatic enteropancreatic neuroendocrine tumors. N Engl J Med. 2014;371(3):224-33.
25. Yao JC, Shah MH, Ito T, Bohas CL, Wolin EM, Van Cutsem E, et al. Everolimus for advanced pancreatic neuroendocrine tumors. N Engl J Med. 2011;364(6):514-23.

26. Yao JC, Fazio N, Singh S, Buzzoni R, Carnaghi C, Wolin E, et al. Everolimus for the treatment of advanced, non-functional neuroendocrine tumours of the lung or gastrointestinal tract (RADIANT-4): a randomised, placebo-controlled, phase 3 study. Lancet. 2016;387(10022):968-77.
27. Raymond E, Dahan L, Raoul JL, Bang YJ, Borbath I, Lombard-Bohas C, et al. Sunitinib malate for the treatment of pancreatic neuroendocrine tumors. N Engl J Med. 2011;364(6):501-13.
28. JA C, A D, HP S, al. e. Cabozantinib in patients with advanced neuroendocrine tumors: a multicenter, randomized, double-blind, placebo-controlled, phase 3 trial (CABINET). New England Journal of Medicine. 2024;390(5):451-62.
29. Strosberg J, El-Haddad G, Wolin E, Hendifar A, Yao J, Chasen B, et al. Phase 3 Trial of (177)Lu-Dotatate for Midgut Neuroendocrine Tumors. N Engl J Med. 2017;376(2):125-35.
30. Kunz PL, Graham NT, Catalano PJ, Nimeiri HS, Fisher GA, Longacre TA, et al. Randomized Study of Temozolomide or Temozolomide and Capecitabine in Patients With Advanced Pancreatic Neuroendocrine Tumors (ECOG-ACRIN E2211). Journal of Clinical Oncology. 2022;41(7):1359-69.
31. Röntgen WC. Ueber eine neue Art von Strahlen. itzungsberichte der Physikalisch-Medizinischen Gesellschaft zu Würzburg. 1895:137-47.
32. Becquerel H. Sur les radiations émises par phosphorescence. Comptes Rendus de l'Académie des Sciences. 1896;122:420-1.
33. Tretkoff E. Henri Becquerel Discovers Radioactivity. APS News. 2008.
34. Becquerel H. Sur les radiations invisibles émises par les corps phosphorescents. Comptes Rendus de l'Académie des Sciences https://weblemoyneedu/giunta/becquerelhtml. 1896;122:501-3.
35. Livingood JJ, Seaborg GT. A Table of Induced Radioactivities. Reviews of Modern Physics. 1940;12(1):30-46.
36. Lawrence JH. Nuclear Physics and Therapy: Preliminary Report on a New Method for the Treatment of Leukemia and Polycythemia. Radiology. 1940;35(1):51-60.
37. Gear J. Milestones in dosimetry for nuclear medicine therapy. Br J Radiol. 2022;95(1135):20220056.
38. Fahey FH, Grant FD, Thrall JH. Saul Hertz, MD, and the birth of radionuclide therapy. EJNMMI Phys. 2017;4(1):15.
39. Seidlin SM, Marinelli LD, Oshry E. Radioactive iodine therapy: Effect on functioning metastases ofadenocarcinoma of the thyroid. CA: A Cancer Journal for Clinicians. 1990;40(5):299-317.
40. Peterson TE, Furenlid LR. SPECT detectors: the Anger Camera and beyond. Phys Med Biol. 2011;56(17):R145-82.
41. Gottschalk A. The early years with Hal Anger. Semin Nucl Med. 1996;26(3):171-9.
42. Poty S, Francesconi LC, McDevitt MR, Morris MJ, Lewis JS. α-Emitters for Radiotherapy: From Basic Radiochemistry to Clinical Studies—Part 1. Journal of Nuclear Medicine. 2018;59(6):878-84.

43. Stokke C, Kvassheim M, Blakkisrud J. Radionuclides for Targeted Therapy: Physical Properties. Molecules. 2022;27(17).
44. Okuhata K, Monzen H, Nakamura Y, Takai G, Nagano K, Nakamura K, et al. Effectiveness of shielding materials against 177Lu gamma rays and the corresponding distance relationship. Annals of Nuclear Medicine. 2023;37(11):629-34.
45. Pecharsky VK, Gschneidner KA, Jr. rare-earth element. Encyclopedia Britannica2025.
46. Mineral commodity summaries 2025. Report. Reston, VA; 2025. Report No.: 2025.
47. Zapp P, Schreiber A, Marx J, Kuckshinrichs W. Environmental impacts of rare earth production. MRS Bull. 2022;47(3):267-75.
48. Vogel WV, van der Marck SC, Versleijen MWJ. Challenges and future options for the production of lutetium-177. Eur J Nucl Med Mol Imaging. 2021;48(8):2329-35.
49. Dewaraja Y, Sjögreen-Gleisner K. Dosimetry for Radiopharmaceutical Therapy. Vienna: International Atomic Energy Agency; 2023.
50. Khazaei Monfared Y, Heidari P, Klempner SJ, Mahmood U, Parikh AR, Hong TS, et al. DNA Damage by Radiopharmaceuticals and Mechanisms of Cellular Repair. Pharmaceutics. 2023;15(12):2761.
51. Dale R. The Application of the Linear-quadratic Dose-effect Equation to Fractionated and Protracted Radiotherapy. The British journal of radiology. 1985;58:515-28.
52. Mínguez P, Gustafsson J, Flux G, Gleisner KS. Biologically effective dose in fractionated molecular radiotherapy--application to treatment of neuroblastoma with (131)I-mIBG. Phys Med Biol. 2016;61(6):2532-51.
53. Aerts A, Eberlein U, Holm S, Hustinx R, Konijnenberg M, Strigari L, et al. EANM position paper on the role of radiobiology in nuclear medicine. Eur J Nucl Med Mol Imaging. 2021;48(11):3365-77.
54. McMahon SJ. The linear quadratic model: usage, interpretation and challenges. Phys Med Biol. 2018;64(1):01tr.
55. Levine R, Krenning EP. Clinical History of the Theranostic Radionuclide Approach to Neuroendocrine Tumors and Other Types of Cancer: Historical Review Based on an Interview of Eric P. Krenning by Rachel Levine. J Nucl Med. 2017;58(Suppl 2):3s-9s.
56. Krenning EP, Kwekkeboom DJ, Bakker WH, Breeman WA, Kooij PP, Oei HY, et al. Somatostatin receptor scintigraphy with [111In-DTPA-D-Phe1]- and [123I-Tyr3]-octreotide: the Rotterdam experience with more than 1000 patients. Eur J Nucl Med. 1993;20(8):716-31.
57. International Atomic Energy A. LiveChart of Nuclides – Indium-111 (In-111). 2024.
58. Heppeler A, Froidevaux S, Mäcke HR, Jermann E, Béhé M, Powell P, et al. Radiometal-Labelled Macrocyclic Chelator-Derivatised Somatostatin Analogue with Superb Tumour-Targeting Properties and Potential for Receptor-Mediated Internal Radiotherapy. Chemistry – A European Journal. 1999;5(7):1974-81.

59. Viola-Villegas N, Doyle RP. The coordination chemistry of 1,4,7,10-tetraazacyclododecane-N,N′,N″,N‴-tetraacetic acid (H4DOTA): Structural overview and analyses on structure–stability relationships. Coordination Chemistry Reviews. 2009;253(13):1906-25.
60. Waldherr C, Pless M, Maecke HR, Schumacher T, Crazzolara A, Nitzsche EU, et al. Tumor response and clinical benefit in neuroendocrine tumors after 7.4 GBq (90)Y-DOTATOC. J Nucl Med. 2002;43(5):610-6.
61. Paganelli G, Zoboli S, Cremonesi M, Bodei L, Ferrari M, Grana C, et al. Receptor-mediated radiotherapy with 90Y-DOTA-D-Phe1-Tyr3-octreotide. Eur J Nucl Med. 2001;28(4):426-34.
62. Otte A, Herrmann R, Heppeler A, Behe M, Jermann E, Powell P, et al. Yttrium-90 DOTATOC: first clinical results. Eur J Nucl Med. 1999;26(11):1439-47.
63. Valkema R, de Jong M, Bakker WH, Breeman WAP, Kooij PPM, Lugtenburg PJ, et al. Phase I study of peptide receptor radionuclide therapy with [111In-DTPA0]octreotide: The rotterdam experience. Seminars in Nuclear Medicine. 2002;32(2):110-22.
64. Valkema R, Pauwels SA, Kvols LK, Kwekkeboom DJ, Jamar F, de Jong M, et al. Long-Term Follow-Up of Renal Function After Peptide Receptor Radiation Therapy with 90Y-DOTA0,Tyr3</sup>-Octreotide and 177Lu-DOTA0, Tyr3-Octreotate. Journal of Nuclear Medicine. 2005;46(1 suppl):83S-91S.
65. Jong Md, Krenning E. New Advances in Peptide Receptor Radionuclide Therapy. Journal of Nuclear Medicine. 2002;43(5):617-20.
66. European Medicines A. Public summary of positive opinion – orphan designation: Lutetium-177 Lu (n=4710) (tricarboxymethyl-14710 tetraazacyclododec-1-ylacetyl-D-phenylalanyl-L-cysteinyl-L-tyrosyl-D-tryptophanyl-L-lysyl). 2023.
67. Strosberg JR, Caplin ME, Kunz PL, Ruszniewski PB, Bodei L, Hendifar A, et al. (177)Lu-Dotatate plus long-acting octreotide versus high-dose long-acting octreotide in patients with midgut neuroendocrine tumours (NETTER-1): final overall survival and long-term safety results from an open-label, randomised, controlled, phase 3 trial. Lancet Oncol. 2021;22(12):1752-63.
68. Agency EM. Lutathera (INN-lutetium (177Lu) oxodotreotide) – Summary of product characteristics. 2024.
69. Food US, Administration D. Lutathera (lutetium Lu 177 dotatate) – Prescribing Information. 2024.
70. Vegt E, de Jong M, Wetzels JFM, Masereeuw R, Melis M, Oyen WJG, et al. Renal Toxicity of Radiolabeled Peptides and Antibody Fragments: Mechanisms, Impact on Radionuclide Therapy, and Strategies for Prevention. Journal of Nuclear Medicine. 2010;51(7):1049-58.
71. Robbins MEC, Bonsib SM. Radiation Nephropathy: A Review. Scanning Microscopy. 1995;9(2):535-60.
72. Jamar F, Barone R, Mathieu I, Walrand S, Labar D, Carlier P, et al. 86Y-DOTA0)-D-Phe1-Tyr3-octreotide (SMT487)--a phase 1 clinical study: pharmacokinetics, biodistribution and renal protective effect of different regimens of amino acid co-infusion. Eur J Nucl Med Mol Imaging. 2003;30(4):510-8.

73. Imhof A, Brunner P, Marincek N, Briel M, Schindler C, Rasch H, et al. Response, Survival, and Long-Term Toxicity After Therapy With the Radiolabeled Somatostatin Analogue [90Y-DOTA]-TOC in Metastasized Neuroendocrine Cancers. Journal of Clinical Oncology. 2011;29(17):2416-23.
74. Baum RP, Fan X, Jakobsson V, Yu F, Schuchardt C, Chen X, et al. Long-term Nephrotoxicity after PRRT: Myth or Reality. Theranostics. 2024;14(2):451-9.
75. Bodei L, Kidd M, Paganelli G, Grana CM, Drozdov I, Cremonesi M, et al. Long-term tolerability of PRRT in 807 patients with neuroendocrine tumours: the value and limitations of clinical factors. European Journal of Nuclear Medicine and Molecular Imaging. 2015;42(1):5-19.
76. Brabander T, van der Zwan WA, Teunissen JJM, Kam BLR, Feelders RA, de Herder WW, et al. Long-Term Efficacy, Survival, and Safety of [(177)Lu-DOTA(0),Tyr(3)]octreotate in Patients with Gastroenteropancreatic and Bronchial Neuroendocrine Tumors. Clin Cancer Res. 2017;23(16):4617-24.
77. Steinhelfer L, Lunger L, Cala L, Pfob CH, Lapa C, Hartrampf PE, et al. Long-Term Nephrotoxicity of 177Lu-PSMA Radioligand Therapy. Journal of Nuclear Medicine. 2024;65(1):79-84.
78. Schäfer H, Mayr S, Büttner-Herold M, Knorr K, Steinhelfer L, Böger CA, et al. Extensive (177)Lu-PSMA Radioligand Therapy Can Lead to Radiation Nephropathy with a Renal Thrombotic Microangiopathy-like Picture. Eur Urol. 2023;83(5):385-90.
79. Zhang B, Xue L, Wu ZB. Structure and Function of Somatostatin and Its Receptors in Endocrinology. Endocrine Reviews. 2024;46(1):26-42.
80. Baum RP, Zhang J, Schuchardt C, Müller D, Mäcke H. First-in-Humans Study of the SSTR Antagonist (177)Lu-DOTA-LM3 for Peptide Receptor Radionuclide Therapy in Patients with Metastatic Neuroendocrine Neoplasms: Dosimetry, Safety, and Efficacy. J Nucl Med. 2021;62(11):1571-81.
81. Jiang Y, Liu Q, Wang G, Sui H, Wang R, Wang J, et al. Safety and efficacy of peptide receptor radionuclide therapy with 177Lu-DOTA-EB-TATE in patients with metastatic neuroendocrine tumors. Theranostics. 2022;12(15):6437-45.
82. Ballal S, Yadav MP, Tripathi M, Sahoo RK, Bal C. Survival Outcomes in Metastatic Gastroenteropancreatic Neuroendocrine Tumor Patients receiving Concomitant (225)Ac-DOTATATE Targeted Alpha Therapy and Capecitabine: A Real-world Scenario Management Based Long-term Outcome Study. J Nucl Med. 2022.
83. Michler E, Kästner D, Pretze M, Hartmann H, Freudenberg R, Schultz MK, et al. [203/212Pb]Pb-VMT-α-NET as a novel theranostic agent for targeted alpha radiotherapy—first clinical experience. European Journal of Nuclear Medicine and Molecular Imaging. 2025;52(11):4171-83.
84. Delpassand ES, Tworowska I, Esfandiari R, Torgue J, Hurt J, Shafie A, et al. Targeted α-Emitter Therapy with (212)Pb-DOTAMTATE for the Treatment of Metastatic SSTR-Expressing Neuroendocrine Tumors: First-in-Humans Dose-Escalation Clinical Trial. J Nucl Med. 2022;63(9):1326-33.

85. Kratochwil C, Giesel FL, Bruchertseifer F, Mier W, Apostolidis C, Boll R, et al. ^{213}Bi-DOTATOC receptor-targeted alpha-radionuclide therapy induces remission in neuroendocrine tumours refractory to beta radiation: a first-in-human experience. Eur J Nucl Med Mol Imaging. 2014;41(11):2106-19.
86. Claringbold PG, Turner JH. Pancreatic Neuroendocrine Tumor Control: Durable Objective Response to Combination 177Lu-Octreotate-Capecitabine-Temozolomide Radiopeptide Chemotherapy. Neuroendocrinology. 2016;103(5):432-9.
87. Hoogenkamp DS, de Wit–van der Veen LJ, Huizing DMV, Tesselaar MET, van Leeuwaarde RS, Stokkel MPM, et al. Advances in Radionuclide Therapies for Patients with Neuro-endocrine Tumors. Current Oncology Reports. 2024;26(5):551-61.
88. Nonnekens J, van Kranenburg M, Beerens CEMT, Suker M, Doukas M, van Eijck CHJ, et al. Potentiation of Peptide Receptor Radionuclide Therapy by the PARP Inhibitor Olaparib. Theranostics. 2016;6(11):1821-32.
89. Hallqvist A, Brynjarsdóttir E, Krantz T, Sjögren M, Svensson J, Bernhardt P. (177)Lu-DOTATATE in Combination with PARP Inhibitor Olaparib Is Feasible in Patients with Somatostatin-Positive Tumors: Results from the LuPARP Phase I Trial. J Nucl Med. 2025;66(5):707-12.
90. Klubo-Gwiezdzinska J, Van Nostrand D, Atkins F, Burman K, Jonklaas J, Mete M, et al. Efficacy of dosimetric versus empiric prescribed activity of 131I for therapy of differentiated thyroid cancer. J Clin Endocrinol Metab. 2011;96(10):3217-25.
91. Kaminski MS, Tuck M, Estes J, Kolstad A, Ross CW, Zasadny K, et al. 131I-Tositumomab Therapy as Initial Treatment for Follicular Lymphoma. New England Journal of Medicine. 2005;352(5):441-9.
92. Garske-Roman U, Sandstrom M, Fross Baron K, Lundin L, Hellman P, Welin S, et al. Prospective observational study of (177)Lu-DOTA-octreotate therapy in 200 patients with advanced metastasized neuroendocrine tumours (NETs): feasibility and impact of a dosimetry-guided study protocol on outcome and toxicity. Eur J Nucl Med Mol Imaging. 2018;45(6):970-88.
93. Del Prete M, Buteau FA, Arsenault F, Saighi N, Bouchard LO, Beaulieu A, et al. Personalized (177)Lu-octreotate peptide receptor radionuclide therapy of neuroendocrine tumours: initial results from the P-PRRT trial. Eur J Nucl Med Mol Imaging. 2019;46(3):728-42.
94. Emami B, Lyman J, Brown A, Coia L, Goitein M, Munzenrider JE, et al. Tolerance of normal tissue to therapeutic irradiation. Int J Radiat Oncol Biol Phys. 1991;21(1):109-22.
95. Bodei L, Cremonesi M, Ferrari M, Pacifici M, Grana CM, Bartolomei M, et al. Long-term evaluation of renal toxicity after peptide receptor radionuclide therapy with 90Y-DOTATOC and 177Lu-DOTATATE: the role of associated risk factors. European Journal of Nuclear Medicine and Molecular Imaging. 2008;35(10):1847-56.
96. Pauwels S, Barone R, Walrand S, Borson-Chazot F, Valkema R, Kvols LK, et al. Practical dosimetry of peptide receptor radionuclide therapy with (90)Y-labeled somatostatin analogs. J Nucl Med. 2005;46 Suppl 1:92s-8s.

97. Ilan E, Sandstrom M, Wassberg C, Sundin A, Garske-Roman U, Eriksson B, et al. Dose response of pancreatic neuroendocrine tumors treated with peptide receptor radionuclide therapy using 177Lu-DOTATATE. J Nucl Med. 2015;56(2):177-82.
98. Jahn U, Ilan E, Sandström M, Lubberink M, Garske-Román U, Sundin A. Peptide Receptor Radionuclide Therapy (PRRT) with 177Lu-DOTATATE; Differences in Tumor Dosimetry, Vascularity and Lesion Metrics in Pancreatic and Small Intestinal Neuroendocrine Neoplasms. Cancers. 2021;13(5):962.
99. Hebert K, Santoro L, Monnier M, Castan F, Berkane I, Assenat E, et al. Absorbed Dose-Response Relationship in Patients with Gastroenteropancreatic Neuroendocrine Tumors Treated with [(177)Lu]Lu-DOTATATE: One Step Closer to Personalized Medicine. J Nucl Med. 2024;65(6):923-30.
100. Mileva M, Marin G, Levillain H, Artigas C, Van Bogaert C, Marin C, et al. Prediction of (177)Lu-DOTATATE PRRT Outcome Using Multimodality Imaging in Patients with Gastroenteropancreatic Neuroendocrine Tumors: Results from a Prospective Phase II LUMEN Study. J Nucl Med. 2024;65(2):236-44.
101. Maccauro M, Cuomo M, Bauckneht M, Bagnalasta M, Mazzaglia S, Scalorbi F, et al. The LUTADOSE trial: tumour dosimetry after the first administration predicts progression free survival in gastro-entero-pancreatic neuroendocrine tumours (GEP NETs) patients treated with [(177)Lu]Lu-DOTATATE. Eur J Nucl Med Mol Imaging. 2024;52(1):291-304.
102. Ezziddin S, Opitz M, Attassi M, Biermann K, Sabet A, Guhlke S, et al. Impact of the Ki-67 proliferation index on response to peptide receptor radionuclide therapy. Eur J Nucl Med Mol Imaging. 2011;38(3):459-66.
103. Schwartz LH, Litière S, De Vries E, Ford R, Gwyther S, Mandrekar S, et al. RECIST 1.1—Update and clarification: From the RECIST committee. European Journal of Cancer. 2016;62:132-7.
104. Hall EJ, Giaccia AJ. Radiobiology for the radiologist. 6th ed. Philadelphia: Lippincott Williams & Wilkins; 2006. ix, 546 p. p.
105. Garkavij M, Nickel M, Sjogreen-Gleisner K, Ljungberg M, Ohlsson T, Wingardh K, et al. 177Lu-[DOTA0,Tyr3] octreotate therapy in patients with disseminated neuroendocrine tumors: Analysis of dosimetry with impact on future therapeutic strategy. Cancer. 2010;116(4 Suppl):1084-92.
106. Thames HD, Ang KK, Stewart FA, van der Schueren E. Does Incomplete Repair Explain the Apparent Failure of the Basic LQ Model to Predict Spinal Cord and Kidney Responses to Low Doses Per Fraction? International Journal of Radiation Biology. 1988;54(1):13-9.
107. Roth D, Gustafsson J, Sundlöv A, Sjögreen Gleisner K. A method for tumor dosimetry based on hybrid planar-SPECT/CT images and semiautomatic segmentation. Med Phys. 2018;45(11):5004-18.
108. Gustafsson J, Sundlöv A, Sjögreen Gleisner K. SPECT image segmentation for estimation of tumour volume and activity concentration in (177)Lu-DOTATATE radionuclide therapy. EJNMMI Res. 2017;7(1):18.
109. Bland JM, Altman DG. The logrank test. Bmj. 2004;328(7447):1073.

110. Gear JI, Cox MG, Gustafsson J, Gleisner KS, Murray I, Glatting G, et al. EANM practical guidance on uncertainty analysis for molecular radiotherapy absorbed dose calculations. Eur J Nucl Med Mol Imaging. 2018;45(13):2456-74.
111. Nahm FS. Receiver operating characteristic curve: overview and practical use for clinicians. Korean J Anesthesiol. 2022;75(1):25-36.
112. Bates D, Mächler M, Bolker B, Walker S. Fitting Linear Mixed-Effects Models Using lme4. Journal of Statistical Software. 2015;67(1):1 - 48.
113. Robin X, Turck N, Hainard A, Tiberti N, Lisacek F, Sanchez J-C, et al. pROC: an open-source package for R and S+ to analyze and compare ROC curves. BMC Bioinformatics. 2011;12(1):77.
114. Vittinghoff E, McCulloch CE. Relaxing the rule of ten events per variable in logistic and Cox regression. Am J Epidemiol. 2007;165(6):710-8.
115. Kusne Y, Patnaik MM, Halfdanarson TR, Sonbol MB. Therapy-related myeloid neoplasms in 177Lu-DOTATATE treated neuroendocrine tumor patients: how great is the risk? Endocr Relat Cancer. 2025;32(6).
116. Hagmarker L, Svensson J, Ryden T, van Essen M, Sundlov A, Gleisner KS, et al. Bone Marrow Absorbed Doses and Correlations with Hematologic Response During (177)Lu-DOTATATE Treatments Are Influenced by Image-Based Dosimetry Method and Presence of Skeletal Metastases. J Nucl Med. 2019;60(10):1406-13.
117. Persson M, Hindorf C, Ardenfors O, Larsson M, Nilsson JN. Risk of treatment-altering haematological toxicity and its dependence on bone marrow doses in peptide receptor radionuclide therapy. EJNMMI Research. 2024;14(1):13.
118. Bergsma H, van Lom K, Raaijmakers MHGP, Konijnenberg M, Kam BLBLR, Teunissen JJM, et al. Persistent Hematologic Dysfunction after Peptide Receptor Radionuclide Therapy with 177Lu-DOTATATE: Incidence, Course, and Predicting Factors in Patients with Gastroenteropancreatic Neuroendocrine Tumors. Journal of Nuclear Medicine. 2018;59(3):452.
119. Smith-Palmer J, Leeuwenkamp OR, Virk J, Reed N. Lutetium oxodotreotide (177Lu-Dotatate) for the treatment of unresectable or metastatic progressive gastroenteropancreatic neuroendocrine tumors: a cost-effectiveness analysis for Scotland. BMC Cancer. 2021;21(1):10.
120. Strosberg J, El-Haddad G, Wolin E, Chasen B, Kulke M, Bushnell D, et al. Supplementary Appendix: Phase 3 Trial of (177)Lu-Dotatate for Midgut Neuroendocrine Tumors. New England Journal of Medicine. 2017.
121. Thiis-Evensen E, Poole AC, Nguyen H-TT, Sponheim J. Achieving objective response in treatment of non-resectable neuroendocrine tumors does not predict longer time to progression compared to achieving stable disease. BMC Cancer. 2020;20(1):466.
122. Pavel M, Caplin ME, Ruszniewski P, Hertelendi M, Krenning EP, Strosberg JR, et al. Relationship Between Best Tumor Shrinkage and Progression-Free Survival and Overall Survival in Patients With Progressive Midgut Neuroendocrine Tumors Treated With [(177)Lu]Lu-DOTA-TATE: Ad Hoc Analysis of the Phase III NETTER-1 Trial. Cancer Med. 2025;14(9):e70744.

123. Pedraza-Arévalo S, Gahete MD, Alors-Pérez E, Luque RM, Castaño JP. Multilayered heterogeneity as an intrinsic hallmark of neuroendocrine tumors. Reviews in Endocrine and Metabolic Disorders. 2018;19(2):179-92.
124. Schiavo Lena M, Partelli S, Castelli P, Andreasi V, Smart CE, Pisa E, et al. Histopathological and Immunophenotypic Changes of Pancreatic Neuroendocrine Tumors after Neoadjuvant Peptide Receptor Radionuclide Therapy (PRRT). Endocr Pathol. 2020;31(2):119-31.
125. Alipour R, Jackson P, Bressel M, Hogg A, Callahan J, Hicks RJ, et al. The relationship between tumour dosimetry, response, and overall survival in patients with unresectable Neuroendocrine Neoplasms (NEN) treated with (177)Lu DOTATATE (LuTate). Eur J Nucl Med Mol Imaging. 2023;50(10):2997-3010.
126. Kayal G, Roseland ME, Wang C, Fitzpatrick K, Mirando D, Suresh K, et al. Multicycle Dosimetric Behavior and Dose-Effect Relationships in [(177)Lu]Lu-DOTATATE Peptide Receptor Radionuclide Therapy. J Nucl Med. 2025;66(6):900-8.
127. Jahn U, Ilan E, Sandstrom M, Lubberink M, Garske-Roman U, Sundin A. Peptide Receptor Radionuclide Therapy (PRRT) with (177)Lu-DOTATATE; Differences in Tumor Dosimetry, Vascularity and Lesion Metrics in Pancreatic and Small Intestinal Neuroendocrine Neoplasms. Cancers (Basel). 2021;13(5).
128. Hummelshøj NE, Gronbaek H, Bager P, Tabaksblat E, Dam G. Fatigue and quality of life in patients with neuroendocrine neoplasia. Scandinavian Journal of Gastroenterology. 2023;58(1):45-53.
129. Wong RK, Lajkosz K, Myrehaug SD, Brierley J, Laidley D, Juergens R, et al. Does Tumor Response Correlate With Quality of Life Changes Following Lu177DOTATATE Therapy for Neuroendocrine Tumors? Observations From a Multicenter Prospective Study (NCT02743741). International Journal of Radiation Oncology, Biology, Physics. 2021;111(3):e81-e2.
130. Ohlsson H, Gålne A, Trägårdh E, Malmström M, Sundlöv A, Almquist M. Relationship between somatostatin receptor expressing tumour volume and health-related quality of life in patients with metastatic GEP-NET. J Neuroendocrinol. 2022;34(6):e13139.
131. Shi C, Morse MA. Mechanisms of Resistance in Gastroenteropancreatic Neuroendocrine Tumors. Cancers. 2022;14(24):6114.
132. Asp P, Sjögreen-Gleisner K, Fröss-Baron K, Sandström M, Hallqvist A, Bernhardt P, et al. START-NET: Systemic Targeted Adaptive Radiotherapy of Neuroendocrine Tumors (C) – An open-label, multi-center randomised phase III trial comparing safety and efficacy of personalised vs non-personalised radionuclide therapy with 177Lu-DOTATOC. ENETS Annual Conference. 2024.
133. Roth D, Gustafsson J, Warfvinge CF, Sundlov A, Akesson A, Tennvall J, et al. Dosimetric Quantities in Neuroendocrine Tumors over Treatment Cycles with (177)Lu-DOTATATE. J Nucl Med. 2022;63(3):399-405.
134. Peterson AB, Wang C, Wong KK, Frey KA, Muzik O, Schipper MJ, et al. 177Lu-DOTATATE Theranostics: Predicting Renal Dosimetry From Pretherapy 68Ga-DOTATATE PET and Clinical Biomarkers. Clin Nucl Med. 2023;48(5):393-9.

135. Bruvoll R, Blakkisrud J, Mikalsen LT, Connelly J, Stokke C. Correlations between [(68)Ga]Ga-DOTA-TOC Uptake and Absorbed Dose from [(177)Lu]Lu-DOTA-TATE. Cancers (Basel). 2023;15(4).
136. Stenvall A, Gustafsson J, Larsson E, Roth D, Sundlov A, Jonsson L, et al. Relationships between uptake of [(68)Ga]Ga-DOTA-TATE and absorbed dose in [(177)Lu]Lu-DOTA-TATE therapy. EJNMMI Res. 2022;12(1):75.
137. Akhavanallaf A, Peterson AB, Fitzpatrick K, Roseland M, Wong KK, El-Naqa I, et al. The predictive value of pretherapy [(68)Ga]Ga-DOTA-TATE PET and biomarkers in [(177)Lu]Lu-PRRT tumor dosimetry. Eur J Nucl Med Mol Imaging. 2023;50(10):2984-96.
138. Pauwels E, Cleeren F, Tshibangu T, Koole M, Serdons K, Boeckxstaens L, et al. 18F-AlF-NOTA-Octreotide Outperforms 68Ga-DOTATATE/NOC PET in Neuroendocrine Tumor Patients: Results from a Prospective, Multicenter Study. Journal of Nuclear Medicine. 2023;64(4):632-8.

Image Credit

Figure 1. *Micrograph of a pancreatic neuroendocrine tumor (very high magnification; H&E stain).* Image by Nephron, CC BY-SA 4.0, via Wikimedia Commons.

Figure 3. Printed with permission from copyright holder Barbara Hertz, daughter of the late Dr. Saul Hertz, who generously shared the photo of Dr Hertz' notebook.

Printed by Media-Tryck, Lund 2026 NORDIC SWAN ECOLABEL 3041 0903

LUND UNIVERSITY

FACULTY OF MEDICINE

Department of Clinical Sciences

Lund University, Faculty of Medicine
Doctoral Dissertation Series 2026:3
ISBN 978-91-8021-801-6
ISSN 1652-8220